JAMES | Journal of Advances in Modeling Earth Systems

RESEARCH ARTICLE
10.1029/2023MS004096

Spatial Dispersion and Statistical Description of Organized Cumulus Cloud Ensembles in Radiative Convective Equilibrium

J. Savre[1]

[1]Meteorological Institute, Ludwig-Maximilians-Universität, Munich, Germany

Key Points:

- Assuming only marginal cloud-cloud interactions, organized cloud ensembles in radiative convective equilibrium can be modeled using heterogeneous spatial point processes
- At scales smaller than 5 km, fluctuations in total mass flux are dominated by the variability in cloud mass flux
- At scales larger than 5 km, fluctuations in total mass flux are mostly controlled by the spatial variability in cloud count

Supporting Information:

Supporting Information may be found in the online version of this article.

Correspondence to:

J. Savre,
julien.savre@lmu.de

Citation:

Savre, J. (2024). Spatial dispersion and statistical description of organized cumulus cloud ensembles in radiative convective equilibrium. *Journal of Advances in Modeling Earth Systems*, *16*, e2023MS004096. https://doi.org/10.1029/2023MS004096

Received 27 OCT 2023
Accepted 20 MAR 2024

Abstract Descriptions of cloud ensembles in radiative convective equilibrium (RCE) rely mostly on the assumption that clouds are randomly distributed in space, a hypothesis that obviously fails in presence of strong organization. In this work, idealized RCE simulations at horizontal grid spacings ranging from 2 km to 125 m are analyzed, displaying a transition between complete randomness at coarse resolution to a high degree of cold pool driven organization at high resolution. The objective is then twofold: (a) characterizing the spatial cloud patterns focusing on correlation scales and association with covariates; (b) providing a statistical description of organized cloud ensembles to generalize existing theories based on complete randomness. It is demonstrated that organized cloud ensembles may be treated as heterogeneous point processes where individual clouds do not interact substantially with their neighbors. In other words, clouds may be considered as randomly distributed if we restrict the space to regions of high cloud density. In addition, it is shown that in highly organized situations local cloud counts may be modeled using negative binomial distributions, while cloud mass fluxes follow lognormal distributions. The total mass flux within regions of varying sizes can then be predicted by compounding the two aforementioned distributions. The total mass flux variability at scales $\lesssim$5 km is dominated by the heavy-tails of the mass flux distributions, whereas at scales $\gtrsim$5 km, it is entirely controlled by the spatial cloud count variability (the spatial cloud pattern). These results have important implications for the parameterization of organized convection in quasi-equilibrium.

Plain Language Summary Convective clouds play a primary role in the Earth's energy budget and global hydrologic cycle. As such, it is of key importance that climate and weather forecast models are capable of accurately representing the impact of convection on the general state of the atmosphere. Unfortunately, convective clouds can only be explicitly represented in models using grid spacings $\lesssim$2 km. At coarser resolutions, moist convection is an unresolved process that needs to be represented using dedicated parameterizations. These latter typically aim at capturing the collective effect of many convective clouds, but ignore how these clouds are spatially distributed. The spatial cloud distribution is however presumed to have many important consequences on climate sensitivity, and on the intensity of convective events. This work is aimed at providing guidance as to how the spatial distribution of clouds should be parameterized in general atmospheric models. To this end, we rely on idealized high-resolution numerical simulations of tropical convection in equilibrium with its large-scale environment, and propose a thorough analysis of the spatial patterns observed in the simulated cloud ensembles. A statistical model capable of capturing the main properties of organized cloud populations across scales is finally presented.

1. Introduction

Atmospheric moist convection is one of the main drivers of the Earth's general circulation, as well as a key element of the global hydrologic cycle. As a process that is so important for our climate, it is of prime importance to utilize adequate parameterizations capable of precisely representing the impact of subgrid convection in general circulation models or numerical weather prediction systems. Despite continuous advances and the emergence of approaches that are more sophisticated and skillful than ever (Rio et al., 2019), atmospheric convection is still an extremely complex multi-scale process that remains a challenge for modelers.

One particularly active area of research concerns the explicit inclusion of cloud organization in convection parameterizations (Mapes & Neale, 2011; Moncrieff et al., 2017; Yang et al., 2022). Traditional parameterizations based on the mass flux concept (Arakawa & Schubert, 1974; Yanai et al., 1973) generally only aim at representing the collective impact of clouds developing at the subgrid scales in response to a given large scale forcing. These

schemes were designed under the hypothesis that the model grid is sufficiently coarse to contain a large number of clouds. This idea has however been questioned in recent years, in part due to the constant increase in available computational power allowing the models to be run operationally at smaller horizontal grid spacing, but also because of the increasingly large body of literature reporting the importance of convective organization on climate sensitivity (Bony et al., 2015; Hohenegger & Stevens, 2016; Mauritsen & Stevens, 2015) or rainfall intensity (Pendergrass et al., 2016; Tan et al., 2015). Today, recent developments and the emergence of stochastic approaches describing the subgrid population of clouds (Bengtsson et al., 2013; Hagos et al., 2018; Keane et al., 2014; Khouider et al., 2010; Plant & Craig, 2008; Sakradzija et al., 2016) offer the prospect to explicitly include information on spatial convective organization at the subgrid scales. Nevertheless, and although this remains an unrealistic assumption, the majority of existing convective parameterizations, even stochastic ones, still rely on the idea that individual clouds in larger ensembles are randomly distributed in space (Craig & Cohen, 2006; Keane et al., 2014; Plant & Craig, 2008; Sakradzija et al., 2016; Shin & Park, 2020).

Of course, designing parameterizations able to account for the influence of convective organization necessarily involves gaining an in-depth understanding of the processes driving it. In this context, the development and use of high-resolution Cloud Resolving Models (CRMs) proved to be an important breakthrough. CRMs may indeed be configured to simulate idealized states of the atmosphere using grid spacings small enough to resolve individual convective updrafts, which enables one to isolate the processes responsible for convective organization without having to worry about complicating factors such as surface heterogeneities or temporal fluctuations in synoptic forcing. CRMs have for example, been found to be convenient tools to investigate the organization of tropical convection developing under RCE (Bretherton et al., 2005; Held et al., 1993; Holloway & Woolnough, 2016; Jeevanjee & Romps, 2013; Muller & Bony, 2015; Muller & Held, 2012; Savre & Craig, 2023b; Tompkins, 2001a, 2001b; Tompkins & Craig, 1998; Wing et al., 2020). Under such conditions, and even in the absence of significant vertical wind shear, the development of cumulus clouds and their spatial organization is indeed strongly constrained by the dynamics of cold pools (Feng et al., 2015; Jeevanjee & Romps, 2013; Tompkins, 2001a) and the distribution of atmospheric vapor, in particular in large numerical domains allowing the development of large scale moisture inhomogeneities (Holloway & Woolnough, 2016; Muller & Bony, 2015; Tompkins, 2001b).

In the continuity of the studies cited previously, this work proposes to use high-resolution CRM simulations of tropical convection in RCE to provide a detailed statistical description of organized cloud ensembles. By varying the model's horizontal grid size from 2 km to 125 m, a clear transition between random to strongly organized convection can be observed. Whereas the coarser resolution employed in this study was used in the past to evaluate an early statistical theory of convective cloud ensembles (Cohen & Craig, 2006; Davoudi et al., 2010), this work concentrates on the highly organized cloud ensembles obtained at the highest resolutions. It is important to emphasize here that due to the equilibrium setting, homogeneous forcing and relatively small domain size employed (128×128 km^2), the focus of this work is on cold pool driven organization occurring at scales <100 km as described for example, by Tompkins (2001a), which is noticeably different from convective self-aggregation (Muller & Bony, 2015; Muller & Held, 2012; Yanase et al., 2020) and organized mesoscale convective systems (Houze, 2004).

Our objective is then twofold. First, we wish to characterize more accurately the properties of spatial cumulus cloud patterns observed in organized RCE simulations by making use of statistical techniques commonly employed to analyze spatial point patterns (Baddeley et al., 2015; Diggle, 2014). In this context, it is customary to compare empirical spatial patterns to the homogeneous Poisson point process (HPPP), a convenient mathematical model giving rise to complete spatial randomness. In a HPPP, N points are randomly placed in a two-dimensional region B, the probability that exactly N points exist in B being given by a Poisson distribution:

$$f_P(n = N; \lambda) = \frac{(\lambda |B|)^N}{N!} e^{-\lambda |B|} \tag{1}$$

λ representing the intensity of the HPPP and $|B|$ being the area of B. In a HPPP, it is further required that each location have the same probability to support a point, that is λ is independent of space. Since organized convection departs from this ideal HPPP model, we wish to further characterize the extent to which cloud patterns differ from it. In particular, departures from a pure HPPP may be the result of either N obeying a different law of probability than Equation 1, and/or the intensity λ being a function of space (as in an inhomogeneous HPPP). In this latter

case, it may be especially interesting to evaluate the spatial scales at which λ varies, and whether these variations stem from direct cloud-cloud interactions (λ depends directly on the presence and position of other clouds) or inhomogeneities in the generative point process. In the latter case, λ is independent of the position of other clouds, but may be expressed as a function of space or any spatially varying covariate controlling the occurrence of convection (like strong Sea Surface Temperature gradients determine the distribution of moist convection across the Inter-Tropical Convergence Zone).

The second objective concerns the development of a statistical description of organized cloud ensembles in RCE that may serve as a basis for the design of improved parameterizations for organized convection. In particular, placing this study in the context of stochastic mass flux schemes (Plant & Craig, 2008; Sakradzija et al., 2016), two key pieces of information that need to be considered are the distribution of individual cloud mass fluxes in convective cloud ensembles, as well as the spatial arrangement of clouds determining the amount of convective events found within subregions of predefined sizes (representing in practice the grid columns of a host model). Combining these two considerations, and assuming that the cloud ensembles are globally in a state of quasi-equilibrium (Arakawa & Schubert, 1974), the proposed statistical model should thus be capable of representing the variability in total mass flux locally observed within subsets of an organized cloud ensemble.

The manuscript is organized around these two objectives as follows. First, the modeling setup and numerical experiments are described in Section 2. The spatial distribution of clouds is analyzed in Section 3, where the properties of the generative spatial point process giving rise to the simulated cloud patterns are thoroughly investigated. Section 4 then describes and evaluates a statistical model capable of capturing the main statistical properties of the simulated cloud ensembles across scales. Finally, a brief discussion on possible applications of our results is given in Section 5 and conclusions are drawn in Section 6.

2. Modeling Approach and Dataset

The present study relies on simulations in RCE performed using the MISU-MIT Cloud and Aerosol (MIMICA) model (Savre et al., 2014). The complete data set was already introduced in Savre and Craig (2023b) (SC23 in the following) and is only briefly recalled hereafter. A more comprehensive description of the numerical setup is provided as Text S1 in Supporting Information S1).

The general model configuration was designed to replicate the simulations presented in Cohen and Craig (2006). The numerical domain extends over 128 km in both horizontal directions, with a domain top situated 18 km above the surface. Note that such a small domain size is expected to prevent the emergence of convective self-aggregation, the onset of which being generally observed at resolutions exceeding 2 km and with domain sizes larger than ∼200 km (Muller & Held, 2012; Yanase et al., 2020). It should therefore be kept in mind that the mode of organization discussed throughout this paper differs from classical convective self-aggregation and is primarily controlled by cold pool dynamics. Initial potential temperature and water vapor profiles were taken from Jordan (1958) while horizontal winds were initially set to 0 m s^{-1} everywhere. The sea surface temperature was held constant in space and time at 300 K. Convection is forced by imposing a time independent cooling rate (no interactive radiation) that remains constant and equal to -2 K d^{-1} below 400 hPa, and decreases linearly to 0 K d^{-1} at 200 hPa. This cooling emulates a net radiative flux of -122 W m^{-2}. Additional configuration details include the use of a Rayleigh damping layer above 16 km, nudging of the horizontal winds with a time scale of 12 hr, and the use of the two-class microphysics scheme described by Grabowski (1998).

Five sets of simulations were performed by progressively decreasing the horizontal grid spacing from $\Delta x = \Delta y = 2$ km to $\Delta x = \Delta y = 125$ m. For the sake of consistency, the vertical grid spacing was kept constant in all cases and equal to 150 m. Since cold pools, which to a large extent control the organization of the cloud population in this situation (Tompkins, 2001a), are on average ≤500 m deep over tropical Oceans (de Szoeke et al., 2017), we cannot expect their vertical structure to be sufficiently well resolved on the chosen grid. Although the sensitivity of our results to vertical resolution was not tested, accurately representing the structure of cold pools and their bulk properties remains of secondary importance in this study as long as convective initiation along cold pool gust fronts and the subsequent organization of the cloud population are captured in a consistent manner across all five experiments. Note besides that Lebo and Morrison (2015) and Squitieri and Gallus (2022) found that simulations of cold pool driven Mesoscale Convective Systems using varying vertical grid lengths in the boundary layer produced qualitatively similar results, a conclusion that is expected to be particularly true over idealized surfaces where the sensitivity of the boundary layer structure to surface fluxes is reduced.

Each simulation at resolutions finer than 2 km was produced by restarting the model from the equilibrium state obtained at the previous resolution doubling the number of grid points in both x and y. When restarting, the model data was always linearly interpolated from the previous coarse grid onto the new finer grid. Whereas the control run at 2 km resolution was run for 45 days to reach this equilibrium, continuing the simulations at subsequent resolutions for 15 days was found to be sufficient to reach a new equilibrium. In each case, it was verified that a new equilibrium was achieved by visually controlling time series of surface fluxes, surface precipitation and cloud fraction at 1,275 m. Once a new equilibrium was reached, horizontal slices were extracted every 1 hr at various altitudes (75 m, 1,275 m, 2,475 m, 5,025 m and 8,025 m) during a period varying from 15 days at 2 and 1 km resolution, to 10 days at 500 m resolution, and 5 days at 250 and 125 m resolution. A large ensemble of instantaneous cloud snapshots was thus available in each case, from 360 at 2 and 1 km, to 120 at 125 and 250 m.

The analysis required the identification of individual clouds within instantaneous model outputs. All clouds were defined at an altitude of 1,275 m (which guaranteed that a majority of all shallow and deep clouds were sampled) as clusters of grid points for which $q_l > 0.001$ g kg^{-1} and $w > 1$ m s^{-1} (q_l being the condensed water mass mixing ratio and w the vertical velocity). As discussed in Appendix A, identifying clouds at higher altitudes did not result in major differences in the clouds spatial distribution and its parameterization despite excluding more than half of the overall cloud population (the shallowest clouds) from the analysis. Only four-point connectivity was considered. This method is similar to that used in SC23.

The choice of using combined thresholds in q_l and w was made keeping in mind that this study is primarily concerned with the design of a statistical representation of convective mass flux variability in organized cloud scenes. Other cloud identification criteria were tested, varying the q_l and w thresholds within reasonable bounds, but no notable change to the results presented here was found. More substantial differences were obtained when defining clouds based on a unique q_l threshold, in which case clouds were found to be generally more numerous, on average larger, but the statistical properties of the cloud ensembles were found to remain largely unaffected (see Text S2 in Supporting Information S1).

3. Cloud Spatial Distribution

3.1. Summary Statistics

As reported in SC23, cloud ensemble statistics obtained in the control simulation with $\Delta x = \Delta y = 2$ km are consistent with the equilibrium statistical mechanics theory formulated by Craig and Cohen (2006) and Cohen and Craig (2006). At this relatively coarse resolution, we may indeed consider that clouds do not interact directly, and that they are randomly distributed in space (Figure 1a).

When horizontal resolution is refined, the mean number of clouds per scene increases, each individual cloud becoming on average smaller and having a weaker mass flux (Prein et al., 2021; Savre & Craig, 2023b; Sueki et al., 2019). The most notable impact of grid refinement on the simulated cloud ensembles is the simultaneous and progressive increase in the degree of spatial organization (Figures 1b–1e). The enhanced organization is accompanied by an increase in the mean size of cold pools, cold pools and convection organization being to a large extent interdependent in such configurations (Feng et al., 2015; Khairoutdinov et al., 2009; Tompkins, 2001a).

Figure 2, displaying the sensitivity of several organization indices to horizontal grid length, confirms these general observations. *SCAI* (the Simple Convective Aggregation Index, Tobin et al. (2012), defined as the product of the scaled number of clouds by the arithmetical mean distance between cloud centroids, here multiplied by a factor 100 instead of 1,000) decreases continuously with increasing resolution, thus suggesting that the cloud population tends to a more aggregated state at high resolution: when reducing the grid length, the amount of clouds identified increases slower than the mean distance between clouds decreases, which indicates that individual cloud cores are more clustered and have the tendency to merge more frequently (SC23). Meanwhile, the subsidence fraction f_{sub}, here defined as the fraction of the domain where the subsidence velocity at an altitude of 2,500 m averaged over 12 hr remains smaller than -0.1 m s^{-1} (definition adapted from Coppin and Bony (2015)), increases with resolution indicating that persistent cloud-free areas, presumably associated with recovering cold pools, cover a larger fraction of the domain at high resolution. Finally, Figure 2 also displays the organization index R_{CE}, often referred to as the Clark-Evans index (Baddeley et al., 2015), and defined as:

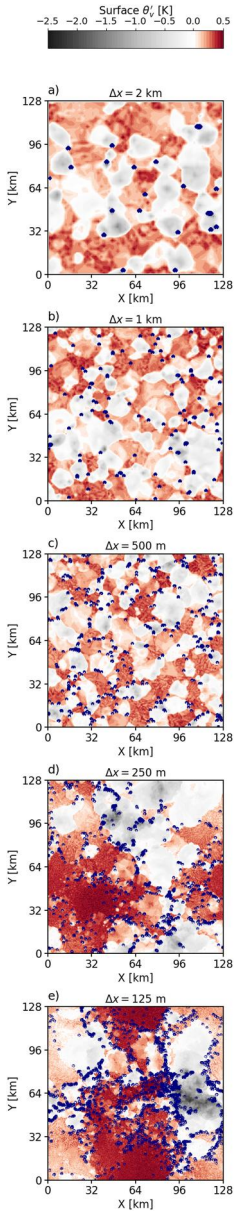

Figure 1. Instantaneous snapshots of surface virtual potential temperature anomalies (θ'_v) at horizontal resolutions of, from top to bottom, 2 km, 1 km, 500 m, 250 m and 125 m. Individual cloud objects identified at 1,275 m are depicted as dark blue contours.

$$R_{CE} = 1 - 2\frac{D_{NN}\sqrt{N_t}}{L}, \tag{2}$$

with D_{NN} the mean nearest neighbor distance computed for each individual cloud, $L = 128$ km is the side length of the numerical domain and N_t is the total number of clouds. The factor $L/\left(2\sqrt{N_t}\right)$ here represents the theoretical mean nearest neighbor distance should all clouds be randomly distributed in space according to a HPPP. R_{CE} bears a lot of similarities with the I_{org} index of Tompkins and Semie (2017). Values lower than 0 suggest spatial regularity whereas $R_{CE} > 0$ indicates spatial clustering ($R_{CE} = 0$ for randomly distributed points). R_{CE} is also bounded by 1, corresponding to the extreme situation in which all points aggregate in very dense clusters and the mean nearest neighbor distance tends to 0. Note also that whereas SCAI and f_{sub} were both designed to diagnose the presence of convective self-aggregation at the mesoscales, R_{CE} is a distance based index able to quantify spatial clustering in much more general situations, regardless of scales. In the present case, R_{CE} goes from nearly 0 at 2 km resolution, suggesting a spatially random cloud population, to 0.4 at 125 m resolution indicating a high degree of spatial clustering and confirming that clouds at horizontal grid spacings <1 km are far from being randomly distributed in space.

An analysis of the reasons why decreasing the horizontal grid spacing leads to an increased degree of organization is out of the scope of the present study, but will be addressed in a subsequent paper. At this stage, noticing that cold pools strongly constrain the initiation and occurrence of active convection, we can only speculate that the increased organization observed at smaller grid spacings is the result of an increasingly large number of clouds being forced to develop along structures (the cold pool edges) exhibiting fairly dissimilar patterns across resolutions (see Figure 1). In order to confirm this hypothesis it seems therefore necessary to specifically investigate the mechanisms controlling the cold pool organization and the variety of simulated subcloud layer patterns.

Whereas the summary statistics presented above are useful to give a broad idea of the degree of organization of the cloud ensembles, they are unable to comprehensively characterize the cloud patterns and underlying generative processes. In particular, and as mentioned in introduction, it may be interesting to determine the extent to which the simulated cloud ensembles deviate from pure spatial randomness as well as the characteristic scales associated with these deviations. These two issues are addressed in the following.

3.2. Scale Dependence

Departures from randomness across scales may first be assessed using a quadrat counting method (Baddeley et al., 2015). The method consists in dividing each available 2D slice into identical squares (or blocks) of equal sizes (L_b will denote the side length of each square) and counting the number of cloud centroids falling into each block. The method is similar to the coarse graining approach used in Cohen and Craig (2006), Shutts and Palmer (2007) and SC23. The cloud count mean and variance, denoted $\langle N \rangle$ and $\mathrm{Var}(N)$ respectively, can then be computed as functions of block size, and the variance-to-mean ratio, also known as index of dispersion $I_d = \mathrm{Var}(N)/\langle N \rangle$, can be used to characterize scale dependent deviations from spatial randomness ($I_d = 1$ for a HPPP). This analysis can be supplemented by Pearson's χ^2-test to characterize situations where the mean number of clouds per block significantly deviates from its expectation assuming a spatially homogeneous population, equal to $N_t L_b^2/L^2$.

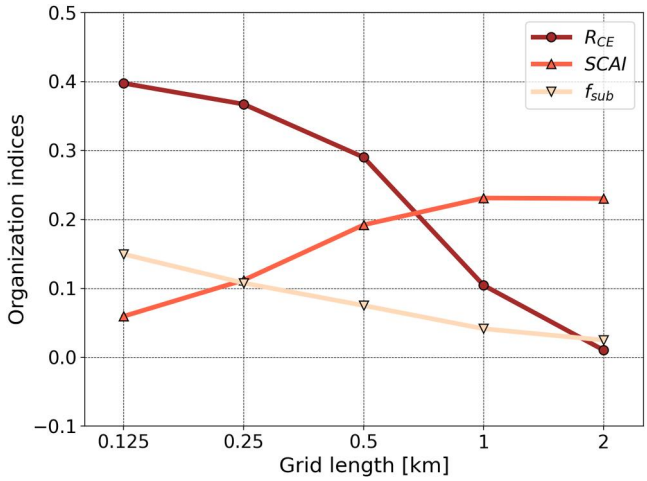

Figure 2. Organization indices as functions of horizontal grid spacing. See text for the definition of each index.

Figure 3 shows the index of dispersion computed for all block sizes possible (from $2\Delta x$ to $L/2$) at each model resolution. The 90% confidence interval is also displayed in each situation. Results from Pearson's χ^2-test are represented on Figure 3 as symbols, where crosses indicate situations in which the null hypothesis that the pattern's intensity λ is homogeneous should be rejected. Acceptance or rejection of the null hypothesis is decided based on an arbitrarily small p-value threshold of 0.01. At 2 km and 1 km resolution, reported I_d values remain generally close to unity, suggesting spatial randomness at all scales. This is confirmed by the χ^2-test p-values indicating that the null hypothesis that λ is spatially homogeneous cannot be rejected at these resolutions. At resolutions $\Delta x \leq 500$ m, I_d generally takes values larger than unity, a sign of spatial clustering. These deviations from spatial randomness are significant at all scales, except for $\Delta x = 500$ m and $L_b > 16$ km. In this situation, the cloud ensemble indeed displays repeated patterns (see Figure 1), possibly owing to the overall smaller cold pools, and resulting in apparent homogeneity at larger scales. Note also that, even at the smallest grid lengths, Pearson's χ^2-test reveals some randomness in the cloud ensembles at $L_b = 2\Delta x$. Care must however be taken when interpreting the test's results at such small block sizes as an insufficient number of clouds per block may alter its significance.

Refined estimates of the scales at which spatial randomness holds may generally be obtained using higher-order statistics such as the pair correlation function (PCF, Stoyan and Stoyan (1994)), all the more so as descriptive statistics like R_{CE} (Section 3.1) or I_d may yield erroneous results under specific conditions (see for example Biagioli and Tompkins (2023)). The PCF, denoted $g(r)$, may be defined as:

$$g(r) = \frac{1}{N_t N_0(r)} \sum_{i}^{N_t} \sum_{j \neq i} \mathbf{1}\{r < d_{ij} \leq r + dr\}. \quad (3)$$

In the above, d_{ij} is the euclidean distance between clouds i and j, dr is a distance interval (which we chose equal to Δx), N_t is the total number of clouds considered and $N_0(r)$ is a normalization factor. Function $g(r)$ corresponds to the normalized mean number of points found between circles of radii r and $r + dr$ centered at each point location. At first, the normalization factor is defined considering that clouds are distributed according to a HPPP, in which case $N_0(r) = 2\pi r dr(N_t - 1)/A$, with A the total area of the domain. It results that $g(r) = 1$ corresponds to the situation where all clouds are randomly distributed in space, $g(r) > 1$ indicates that more clouds than expected are present at a distance r, thus suggesting spatial clustering, whereas $g(r) < 1$ suggests the opposite situation of a regularly distributed cloud population. PCFs have specifically been used to investigate cumulus cloud patterns by Nair et al. (1998), Rasp et al. (2018), and Senf et al. (2019). Alternative higher-order statistics like Besag's L-function (Biagioli & Tompkins, 2023) may also be used in this context and are expected to yield similar results.

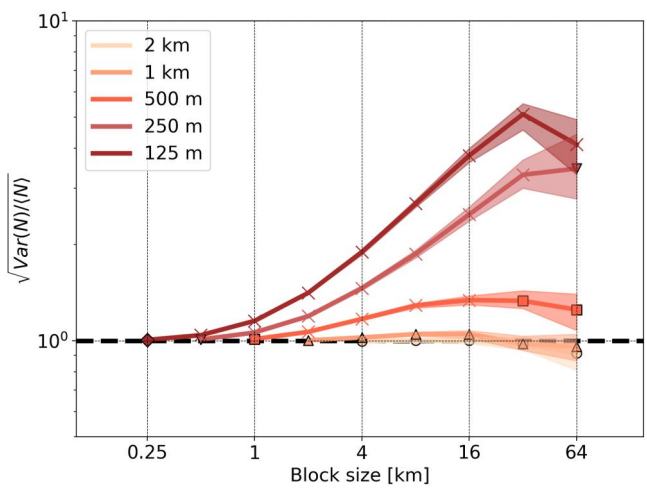

Figure 3. Variance-to-mean ratios (i.e., index of dispersion, I_d) plotted as a function of block size and horizontal resolution. The 90% confidence intervals are represented as areas shaded with colors matching the corresponding lines. Symbols are used to indicate the results of Pearson's χ^2-test applied to cloud counts per block: crosses denote situations in which the null hypothesis that clouds are homogeneously distributed in space should be rejected.

PCFs are shown on Figure 4a for all five numerical experiments. PCFs calculated at resolutions 2 km to 500 m generally behave similarly, with $g(r)$ remaining initially >1 at short distances but quickly decreasing to unity as r is increased. Only at the largest grid spacing of 2 km does the PCF show signs of regularity at distances $r < 30$ km. Short range regularity in the spatial cloud distribution was also noted by Tompkins and Semie (2017) in RCE simulations performed at comparable horizontal grid spacings (though at slightly shorter distances $r < 15$ km), a feature attributed to the repulsive effect of cold pools on nearby clouds. $g(r)$ values larger than 1 at $\Delta x < r < 2\Delta x$, are normal features of PCFs obtained for low-density non-overlapping particles, and do not necessarily indicate clustering at small scales. Values $g(r) > 1$ at scales

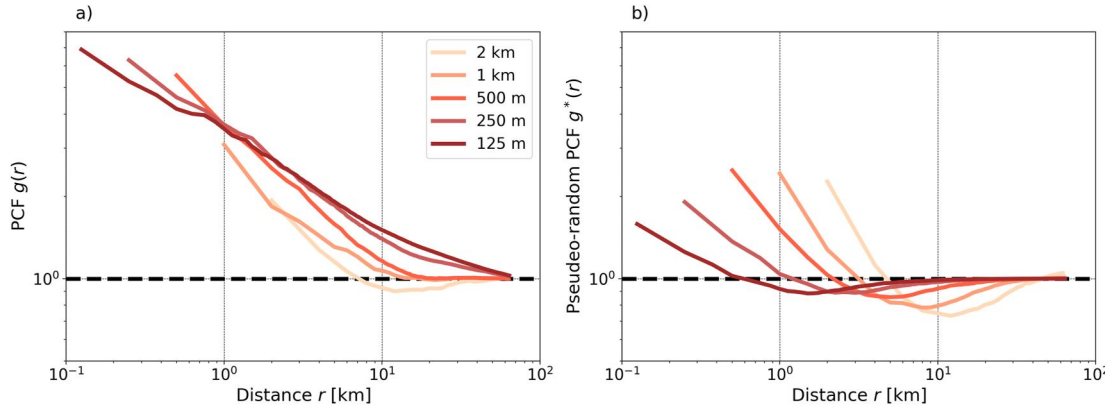

Figure 4. Pair correlation functions (PCFs) calculated for all five numerical experiments and plotted as functions of distance from each cloud's centroid. Panel (a): all clouds are considered and PCFs are normalized assuming clouds are randomly distributed in space, all grid points having the same probability to support a cloud. Panel (b): same as panel (a) except that PCFs are now normalized assuming clouds are pseudo-randomly distributed in space, each grid point being attributed a probability to bear a cloud proportional to the local value of the smoothed intensity $\hat{\lambda}$. According to Equation 3, each data point is obtained after counting the number of clouds found between distances r and $r + dr$ (with $dr = \Delta x$) from each cloud's centroid: the first point of each curve at $r = \Delta x$ therefore contains all clouds situated between Δx and $2\Delta x$ away from each cloud's centroid.

$r > 2\Delta x$ are however strong indicators of clustering, as is the case for example, at $\Delta x = 500$ m up to ∼15 km. This coincides roughly with the homogeneity threshold determined previously based on Pearson's χ^2-test.

At smaller grid spacings no evidence of spatial randomness can be seen, in agreement with Pearson's χ^2-test results. $g(r)$ indeed remains consistently larger than unity at all scales, and only reaches ∼1 at scales ∼$L/2$ where finite domain size effects start to be significant. This behavior is often interpreted as being the result of long-range correlations among clouds. To be more precise, $g(r) > 1$ at all scales indicates that clouds in these cases tend to aggregate in clusters having sizes comparable to the domain length. It must be emphasized however that, at this stage, it is still impossible to confirm whether deviations from spatial randomness stem from direct cloud-cloud interactions or spatial heterogeneities in the intensity of the generative point process, with λ being a one-to-one function of some other variable of the simulated convective field such as surface fluxes or moisture convergence in the boundary layer.

3.3. Association With Covariates

In order to determine the importance of spatial heterogeneities on the simulated cloud patterns, we start by determining whether λ (i.e., the probability to find a cloud at a particular location) is related to some underlying property of the atmosphere (or covariate). Considering the overarching goal of the study consisting in designing a simple statistical framework that may be used in stochastic schemes to describe the spatial organization of convection, we are especially interested in knowing whether λ may be expressed as a monotonic function of variables directly available in large-scale models.

Let's first introduce an empirical cloud intensity field $\hat{\lambda}$, used as a proxy for λ, obtained by applying a Gaussian kernel smoother:

$$\hat{\lambda}(\mathbf{x}) = \sum_{i=1}^{N_t} \mathcal{G}(\mathbf{x} - \mathbf{x}_i), \tag{4}$$

with $\mathbf{x}_i$ the locations of the N_t cloud centroids, and $\mathcal{G}$ a Gaussian kernel of width (standard deviation) σ, centered in $\mathbf{x}_i$. Filled contours in Figure 5 represent the normalized empirical intensity $\hat{\lambda}$ calculated for the cloud fields depicted on Figure 1. On the figure and in the following, we chose to set $\sigma = D_{NN}$ in each case, where D_{NN}, the mean nearest neighbor distance, was defined in Section 3.1. Employing a case dependent kernel was found to be necessary to obtain a smooth intensity field at low cloud densities (as in Figures 5a and 5b where we expect $\hat{\lambda}$ to be nearly constant in space) while preserving the organization patterns seen at higher cloud densities (as in Figures 5d and 5e). Correlations between $\hat{\lambda}$ and predefined covariates ϕ can then be assessed by comparing

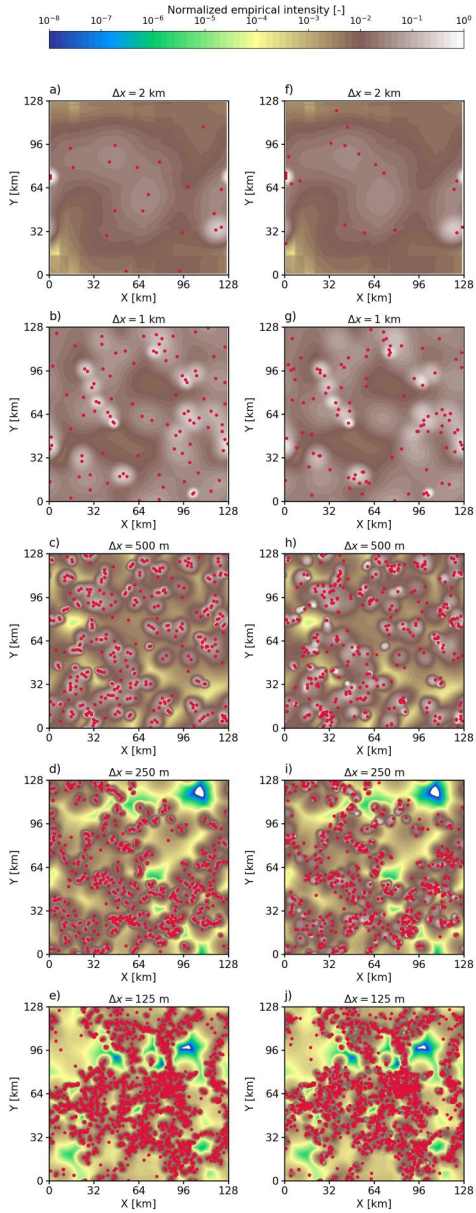

Figure 5. Panels (a–e): same as Figure 1 except that the filled contours now represent the normalized empirical intensity obtained from Equation 4 with red dots indicating the position of each cloud. Panels (f–j): same as panels (a–e) except that each cloud is now pseudo-randomly placed on the grid, associating each grid point with a probably to support a cloud equal to the empirical intensity $\hat{\lambda}$.

covariate cumulative density functions (CDFs) estimated at locations where $\hat{\lambda}$ is larger than its 80th percentile (i.e., in regions of high cloud density), denoted $\hat{F}(\phi)$, to equivalent CDFs estimated at all data points, $F(\phi)$ (Baddeley et al., 2015). When the cloud pattern intensity does not correlate with a given covariate, the total and high cloud density CDFs, should be equal, that is, $F(\phi) = \hat{F}(\phi)$. Situations where $\hat{F} > F$ indicate that high cloud densities are associated with low covariate values, whereas for $\hat{F} < F$, high cloud densities are associated with high covariate values. To further quantify the association between $\hat{\lambda}$ and the considered covariates, we can also calculate the area below the curve $\hat{F}(\phi)$ against $F(\phi)$:

$$I_{cov} = |1 - 2\int_0^1 \hat{F}\{F^{-1}[F(\phi)]\}\, dF(\phi)|. \quad (5)$$

Values of I_{cov} close to 1 then indicate a strong association between $\hat{\lambda}$ and ϕ, while values of 0 suggest complete independence.

Figure 6 displays the CDFs $\hat{F}(\phi)$ plotted against $F(\phi)$ for three horizontal resolutions and four possible covariates thought to impact the development of cumulus clouds: the moist static energy (h) vertically integrated between the surface and a fixed altitude arbitrarily set to z = 825 m (denoted I_h), Latent Heat Fluxes (LHF), the horizontal moisture flux divergence at z = 375 m (Flux q), and virtual potential temperature anomalies at the surface (θ'_v). The upper integration bound for I_h is situated in the lower cloud layer provided that cloud base was found to be located on average 675 m above the surface, with weak spatial and resolution dependency. Additionally, the altitude at which the moisture flux divergence was estimated corresponds roughly to the average cold pool depth, the latter being found to vary between 325 m at 2 km resolution and 350 m at 125 m resolution, consistent with de Szoeke et al. (2017) (cold pools were identified using a θ'_v threshold value of −0.2 K, the cold pool top hence corresponding to the first model level where $\theta'_v > -0.2$ K). I_{cov} values corresponding to the curves displayed on Figure 6 are reported in Table 1.

θ'_v generally emerges as the worst predictor of cloud density independently of resolution with I_{cov} values only marginally larger than 0 (see Figure 6 and Table 1). The fact that $\hat{F}(\theta'_v) \approx F(\theta'_v)$ in all cases indicates that cloud occurrence is largely independent of buoyancy anomalies at the surface. Horizontal moisture advection in the boundary layer also stands out as a particularly inappropriate predictor, this time because Flux q may take either high or low values in high cloud density regions. In contrast LHF and, in particular, I_h correlate much better with cloud density, with high I_h and low LHF values associated with high $\hat{\lambda}$. The predictive power of both LHF and I_h is especially good at 125 m resolution, with I_{cov} values of 0.16 and 0.45 respectively, whereas only weak correlations are found at 2 km resolution, with I_{cov} values as low as 0.12 and 0.03 respectively, consistent with the fact that clouds are nearly randomly and homogeneously distributed in space. Note that a weaker predictive power is found when integrating h through the whole atmosphere, whereas considering the water vapor content instead of h yields very similar results.

In complement, we may again use Pearson's χ^2-test, now defining quadrats based on quantiles of selected covariates instead of using square blocks of varying sizes. Delimiting regions based on covariate quantiles results in the creation of blocks of irregular shapes but equal sizes for which it is easy to determine the expected cloud count in the case of a spatially random and homogeneous cloud population. The fraction of clouds counted within 4 covariate quantiles (using a small amount of quantiles is necessary to guarantee that enough clouds are sampled

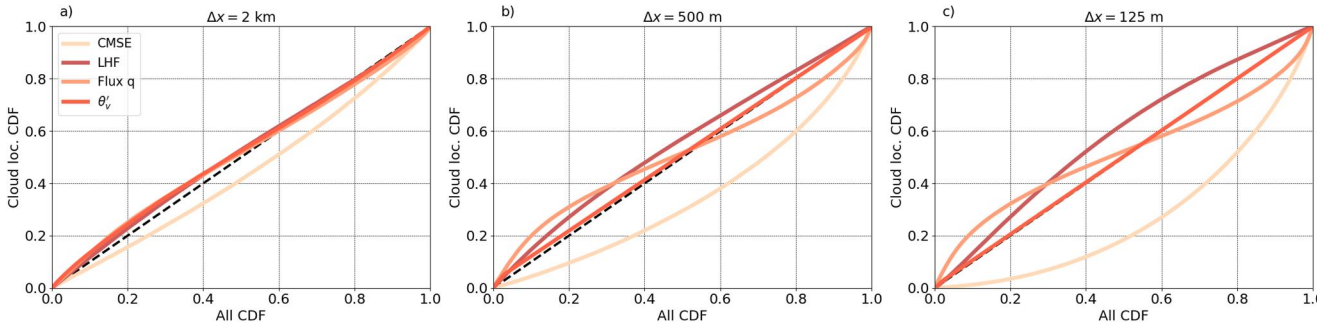

Figure 6. Covariate cumulative density functions (CDFs) estimated in regions where the cloud density $\hat{\lambda}$ exceeds its 80th percentile and plotted as functions of overall covariate CDFs. Four different covariates were tested: CMSE corresponds to the vertically integrated moist static energy (I_h in the text), LHF refers to the surface latent heat fluxes, Flux q is the horizontal moisture convergence at 350 m and θ'_v is the virtual potential temperature anomaly at the surface. Results are plotted for 3 different model resolutions: panel (a), 2 km, panel (b), 500 m and panel (c), 125 m.

within each subregion) are plotted on Figure 7 for the same covariates as those defined previously. As in Figure 3, crosses indicate situations in which the null hypothesis that the cloud population is homogeneously distributed across quantiles should be rejected. The null hypothesis that the cloud population is homogeneously distributed across quantiles is verified at all resolutions when quantiles are estimated from LHF. This implies that the process intensity $\hat{\lambda}$ correlates only weakly with surface fluxes (sensible heat fluxes exhibit the same behavior). The situation is similar when considering θ'_v quantiles, especially at coarse resolutions.

Considering divisions based on I_h and Flux q, spatial heterogeneity clearly dominates at all resolutions, except perhaps for $\Delta x = 2$ km. It should however be noted again that high cloud densities are found in both the upper and lower Flux q quantiles. Provided that high and low Flux q values are associated with strong low level moisture convergence and divergence respectively, we may speculate that the former situation is evidence of local convective initiation, whereas the latter situation may be related to mature convective activity and the formation of cold pools. This confirms that Flux q is not a good cloud count predictor, although |Flux q| might be, with the sign of Flux q giving additional information on the development stage of convection.

Overall, we may speculate that the strong association between $\hat{\lambda}$ and I_h and, to some extent, Flux q hints at the predominant influence of cold pool dynamics on cloud clustering. Moisture indeed converges along cold pool gust fronts thus creating local vapor and h maxima at the edge of the cold pools (Chandra et al., 2018). The mechanical lifting of energetic air parcels along the cold pool fronts then facilitates the initiation of new convective clouds (Feng et al., 2015; Rotunno et al., 1988; Tompkins, 2001a; Torri et al., 2015) which hence explains why higher cloud densities are preferentially found in regions of high I_h.

3.4. Spatial Heterogeneity or Direct Cloud-Cloud Interactions?

The PCFs shown in Section 3.2 can only inform us on increased or decreased cloud occurrence at a certain distance from a reference location (Senf et al., 2019), but they are not able to distinguish between departures from randomness due to intensity heterogeneities or direct cloud-cloud interactions. In order to separate these two effects, we may recalculate the PCF $g(r)$ (Equation 3) using a normalization factor obtained from a synthetic, pseudo-random cloud population exhibiting the same empirical intensity field $\hat{\lambda}$ as the simulated population. The procedure used to calculate the pseudo-random normalization factor, which we denote $N_0^*(r)$ (the corresponding PCF is denoted $g^*(r)$), consists in distributing N_t clouds in space, attributing to each grid point a probability to bear a cloud proportional to the empirical intensity calculated at that point. A similar method using pseudo-randomized cloud populations was employed by Senf et al. (2019). Single instances of such pseudo-random cloud fields are shown on the right column of Figure 5.

Table 1
Covariate Indices I_{cov} for Three Different Resolutions and Four Covariate Variables

Covariates	I_h	LHF	Flux q	*buoy*
$\Delta x = 2$ km	0.12	0.03	0.02	0.04
$\Delta x = 500$ m	0.30	0.10	0.03	0.02
$\Delta x = 125$ m	0.45	0.16	0.03	0

Note. See text for details.

Values of $g^*(r)$ computed in all five simulations are plotted on Figure 4b. As opposed to the standard case (Figure 4a), all pseudo-random PCFs possess the same overall shape independently of resolution. At small scales, $g^*(r) > 1$

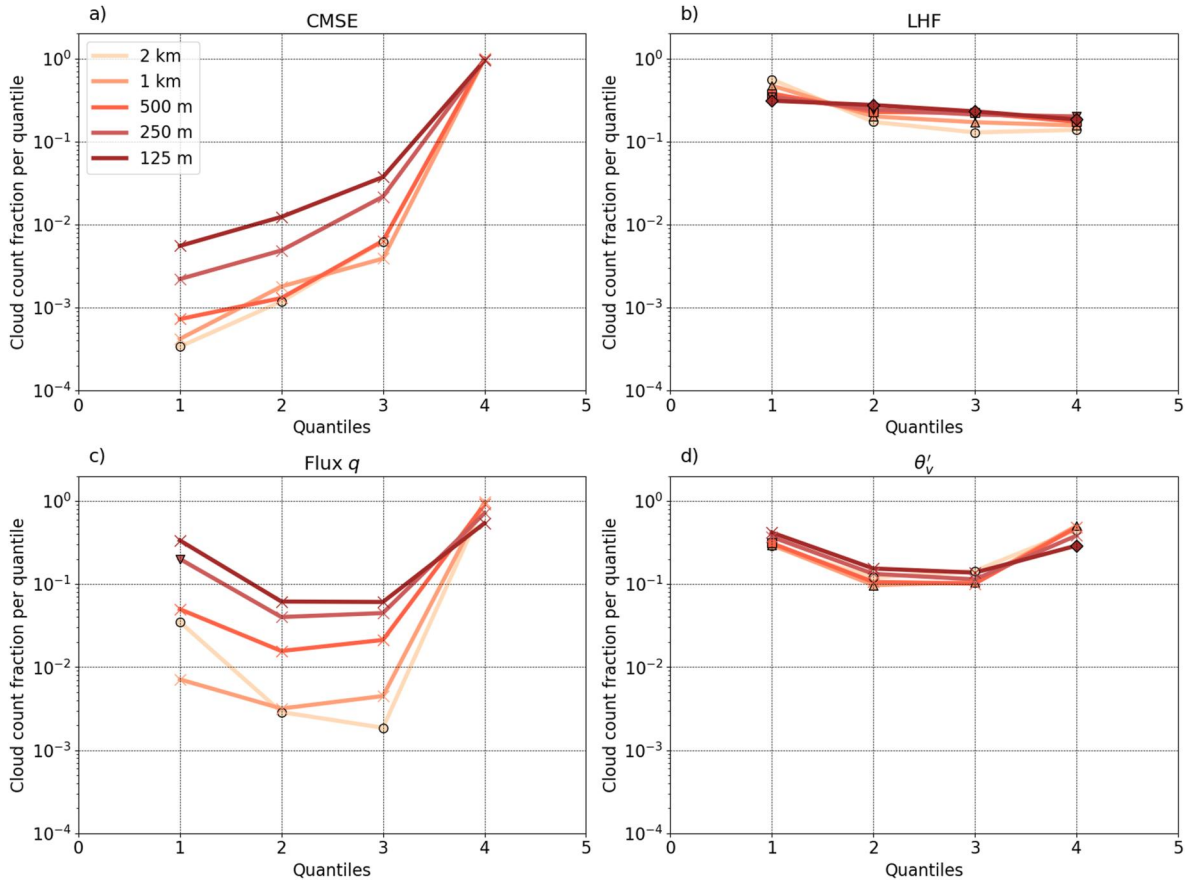

Figure 7. Fraction of cloud amount counted within quadrats defined based on 4 covariate quantiles. Selected covariates are: (a) I_h in the boundary layer, (b) LHF, (c) moisture advection in the middle of the boundary layer (Flux a) and (d) θ_v' in the middle of the boundary layer. Symbols indicate the outcome of Pearson's χ^2-test of homogeneity (crosses are used when the null hypothesis of spatial homogeneity should be rejected).

indicating short range attraction. As mentioned previously, this feature is characteristic of PCFs obtained with hard spheres and reflects the fact that clouds behave as impenetrable objects of finite sizes. At sufficiently large distances (>5 km at 250 and 125 m resolution), $g^*(r) \to 1$ suggesting that clouds develop independently of each other at larger scales: there is no long-range interaction between clouds, especially at fine resolution. Finally, at intermediate scales, $g^*(r) < 1$. This may be interpreted as the direct manifestation of cloud-cloud interactions, suggesting in particular that clouds exert repulsive forces on each other and appear regularly distributed at these scales. We may in particular speculate that convective downdrafts are to a large extent responsible for the creation of regular separations between individual clouds: (a) compensating downdrafts outside active cumuli stabilize the near-cloud environment and therefore prevent other clouds from developing close to the original convective cells, and (b) convective downdrafts penetrating the boundary layer may generate cold pools, sometimes even small ones, thus effectively suppressing the initiation of moist convection in the vicinity of the parent cloud. Perhaps more importantly, Figure 4 gives us estimates at which these direct interactions act: the distance at which $g^*(r)$ reaches a minimum, corresponding to the distance at which repulsion is the strongest, decreases with decreasing grid spacing, taking values of 3 and 1.5 km at 250 m and 125 horizontal grid spacing, respectively.

This analysis thus suggests that direct cloud-cloud interactions in well resolved, organized cloud ensembles are only significant at scales smaller than ∼5 km. At larger scales, the cloud pattern is primarily determined by spatial heterogeneities in boundary layer properties.

It must be noted that although we made the choice to distinguish between the impact of spatial heterogeneities in the atmospheric state and direct cloud-cloud interactions, our results may be interpreted differently by noticing that spatial heterogeneities in the atmospheric state as described in Section 3.3 are also to a large extent controlled by past convective activity (the cold pools that shape the structure of the boundary layer originate from past

convective clouds). This last notion is largely reminiscent of the concept of convective memory studied for example, by Colin et al. (2019), and in particular of what the authors refer to as "microstate memory." Therefore, instead of contrasting intensity heterogeneities and direct cloud-cloud interactions, an equally valid distinction may be made between "deferred interactions" resulting from past convective activity and its memory stored in the atmospheric state, and "coincident interactions" resulting from coexisting clouds able to directly influence each other.

4. Statistical Models

We wish here to design a statistical model capable of representing spatial fluctuations in total mass flux observed in organized cloud ensembles. The goal is to generalize the theoretical approach of Craig and Cohen (2006) in order to include the impact of organization on the cloud ensemble statistics, while remaining at a level of complexity consistent with practical implementations in stochastic parameterizations (Keane et al., 2014; Plant & Craig, 2008; Sakradzija et al., 2015, 2016).

4.1. Cloud Counts

As noted in introduction, complete spatial randomness can generally be modeled by a HPPP according to which the total number of clouds per scene N follows a Poisson distribution of intensity λ (see Equation 1). Poisson distributed cloud counts served as the basis for the theory proposed by Craig and Cohen (2006), where clouds were assumed to behave as independent non-interacting particles.

When population counts exhibit overdispersion (i.e., the count variance is larger than that expected from a Poisson process, as seen on Figure 3), the negative binomial distribution often constitutes an appropriate alternative model (Ver Hoef & Boveng, 2007; Villarini et al., 2010). This distribution may be defined as:

$$f_{NB}(N;r,p) = \frac{\Gamma(N+r)}{N!\Gamma(r)} p^N (1-p)^r \tag{6}$$

with r and p the distribution's parameters, and Γ denoting the gamma function:.

$$\Gamma(x) = \int_0^{+\infty} t^{x-1} e^{-t} dt, \tag{7}$$

with $x > 0$. By analogy with a HPPP, the mean intensity of a population whose count in a finite two-dimensional space B is distributed according to the above equation is equal to $rp/[(1-p)|B|]$ (in units similar to λ, $|B|$ representing the area of B). The negative binomial distribution generally describes the number of successes drawn in Bernoulli trials before a certain number of failures is reached: r represents the number of failures before stopping the draws, and p is the probability of success. In the above, the definition of f_{NB} has been adapted to accept positive real valued r parameters. Note that the Poisson distribution can be seen as a special case of the negative binomial distribution as $r \to +\infty$. The negative binomial distribution has been used to model overdispersed count data in ecology for a very long time (Bliss & Fisher, 1953), and was more recently applied in atmospheric sciences to describe, for instance, the activity of tropical storms in the North Atlantic (Villarini et al., 2010).

Empirical cloud count distributions along with their corresponding fitted Poisson and negative binomial distributions are plotted on Figure 8 at resolutions of 2 km, 500 and 125 m, for block sizes varying from 2 to 32 km. The intensity of the fitted Poisson distributions was simply evaluated using the equality $\lambda = \langle N \rangle / L^2$. For the negative binomial distributions, the parameters $1/r$ and p were estimated using the following relationships:

$$p = 1 - \frac{\langle N \rangle}{\mathrm{Var}(N)} \quad \text{and} \quad r = \frac{\langle N \rangle^2}{\mathrm{Var}(N) - \langle N \rangle}. \tag{8}$$

At 2 km resolution, no negative binomial fit could be obtained since cloud counts do not show any overdispersion. Count data in this case thus closely follows a Poisson distribution, thereby confirming that cloud ensembles at 2 km resolution can be mathematically modeled by a HPPP. With increasing resolution, empirical count data exhibit more spread than what may be expected from Poisson distributed data. In these situations, count data is

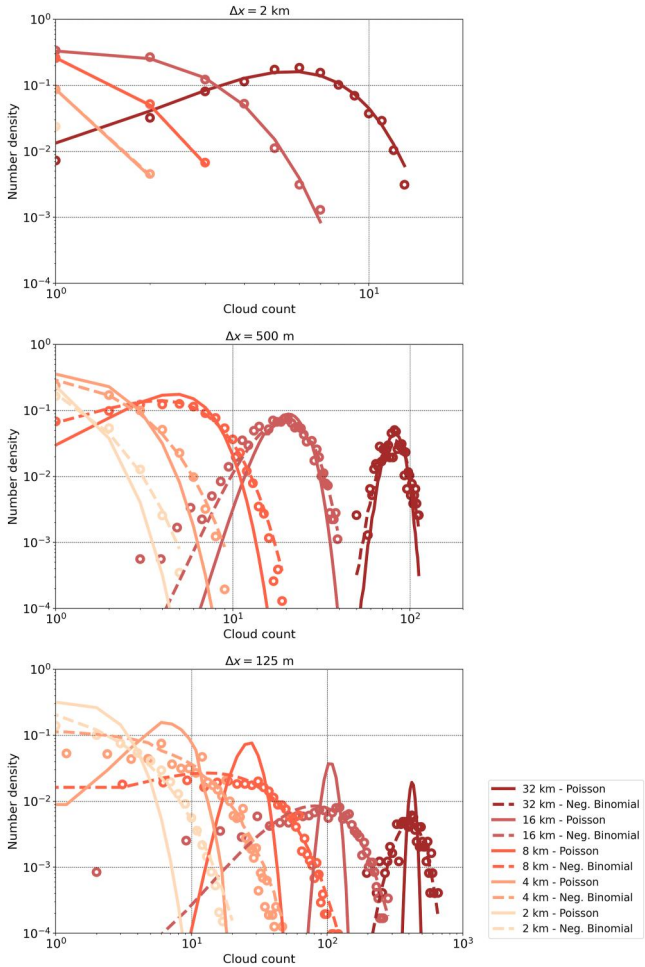

Figure 8. Empirical cloud count distributions (symbols) estimated at 3 different model resolutions (from top to bottom: 2 km, 500 and 125 m), and for block sizes varying between 2 and 32 km. Fitted Poisson and negative binomial distributions are also shown as solid and dashed lines, respectively. Details regarding the evaluation of the distributions parameters λ, $1/r$ and p are given in the main text.

best modeled using negative binomial distributions. This suggests that negative binomial distributions constitute an appropriate choice to model cloud counts in organized cloud populations at various scales.

The negative binomial parameters, $1/r$ and p, are plotted on Figure 9 as functions of block size. At coarse resolution, when cloud counts are relatively well modeled by Poisson distributions, both $1/r$ and p remain close to 0, consistent with the fact that the Poisson distribution is a special case of the negative binomial distribution as $r \to +\infty$. Negative $1/r$ and p values found at these resolutions are unphysical and only reflect the fact that the negative binomial model is inadequate. At high resolution and large block sizes, $1/r$ tends to 0 while p remains close to unity indicating that cloud counts at large scales are close to being Poisson distributed as well. $1/r$ however increases rapidly with decreasing block size whereas p follows the opposite trend and approaches 0 at the smallest scales. In this situation, the number of failures r and, in particular, the probability of success p remain low as the probability to find empty blocks dramatically increases when the blocks become smaller.

Figure 10 further focuses on the dependence of the negative binomial parameters evaluated at 125 m resolution on I_h. Square blocks of varying sizes are here sorted into four categories based on the average I_h values computed within each block. The four categories are then defined as four average I_h quantiles. Note that this quantile classification is different from the quadrat analysis proposed in Section 3.3. The domain was then decomposed into irregular regions based on local I_h values in order to highlight potential correlations between I_h and local cloud density. In contrast, the present method is meant to identify relationships between I_h and negative binomial parameters, provided that the negative binomial distribution is employed to model the number of clouds found within square areas of fixed size. p appears to be relatively independent of I_h, variations in p being primarily controlled by the size of the subregions considered. In contrast, $1/r$ decreases substantially with increasing I_h, and generally even differs by more than one order of magnitude between the lower and upper I_h quantiles. Overall, whereas the probability of success p remains constant throughout the domain and only depends on block size, an increasingly large number of failures r is allowed as I_h is increased.

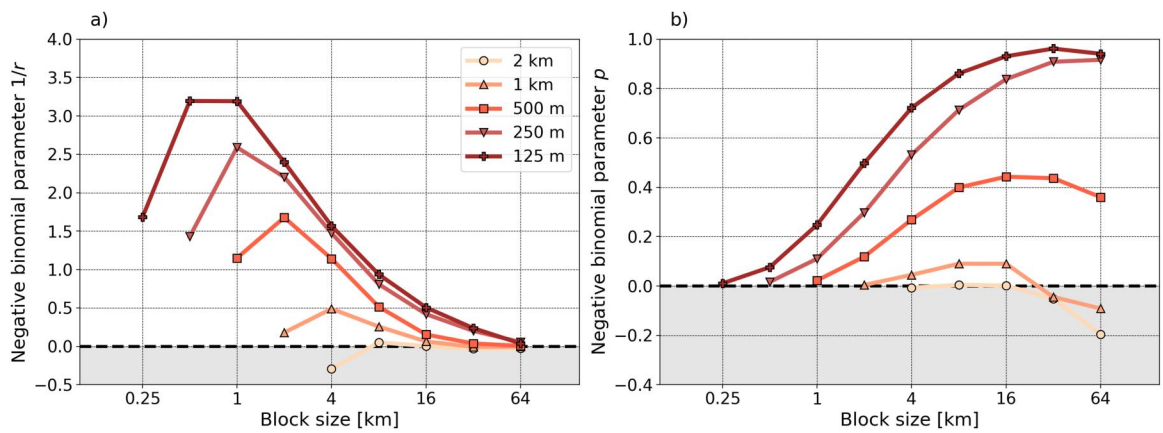

Figure 9. Negative binomial distribution parameters $1/r$ (panel a) and p (panel b) as functions of block size and horizontal resolution. A value $1/r = 0$ corresponds to the Poisson distribution (asymptotically equivalent to the negative binomial distribution as $r \to +\infty$). Negative $1/r$ and p values (gray shaded areas) are mathematically inconsistent. Both p and r were estimated according to Equation 8.

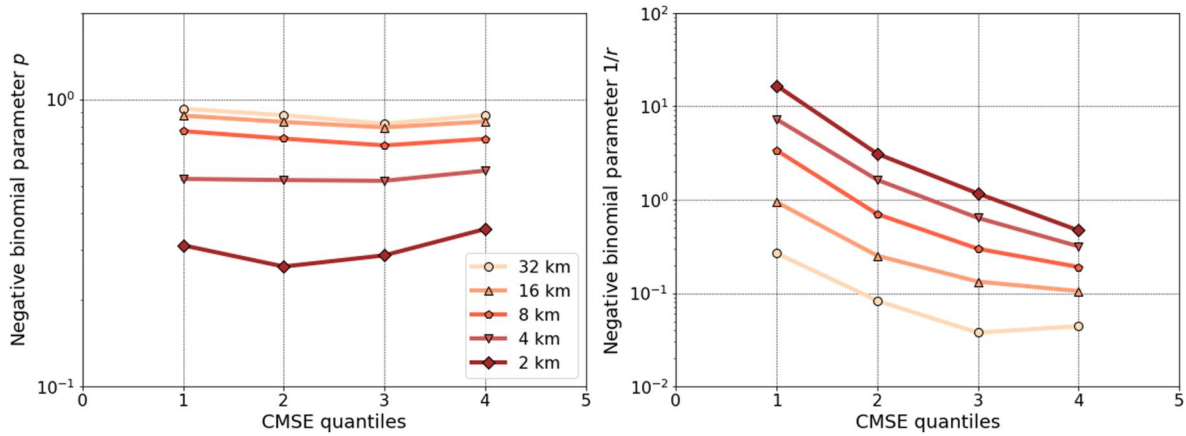

Figure 10. Negative binomial distribution parameter $1/r$ (panel a) and p (panel b) as functions of 4 I_h quantiles, at a unique resolution of 125 m but 5 different block sizes ranging from 2 to 32 km.

In the context of modeling the spatial occurrence of clouds in presence of organization, one may therefore take advantage of these results by using a negative binomial distribution whose parameter r is directly connected to some measure of the boundary layer energetics.

4.2. Cloud Mass Fluxes

Several functional forms have been proposed in the past to represent cloud mass flux distributions. Following Craig and Cohen (2006), and considering a randomly distributed cloud population composed of non-interacting clouds, the principle of maximum entropy predicts that for a fixed, known total mass flux (set by the external forcing strength) the most likely distribution describing individual cloud mass fluxes is an exponential distribution:

$$g_E(m;\langle m\rangle) = \frac{1}{\langle m\rangle} e^{-m/\langle m\rangle}, \tag{9}$$

with $\langle m\rangle$ the mean cloud mass flux. The exponential distribution was shown to accurately model the distribution of mass fluxes in coarse resolution RCE experiments showing no particular sign of organization (Cohen & Craig, 2006).

In organized situations where clouds start to interact strongly, cloud mass flux distributions develop heavy tails which may be modeled using, for example, power-laws (Rasp et al., 2018), Weibull (Sakradzija et al., 2015) or lognormal distributions (LeMone & Zipser, 1980). We follow here SC23 who showed that the global statistical properties of cloud mass fluxes in the present high-resolution RCE experiments are consistent with a lognormal distribution:

$$g_{LN}(m;\mu,\sigma) = \frac{1}{m\sigma\sqrt{2\pi}} \exp\left[-\frac{(\ln m - \mu)^2}{2\sigma^2}\right], \tag{10}$$

with μ and σ the distribution's parameters related to the mean and variance of m. It should be noted that recent studies have suggested that the emergence of heavy tails in cloud mass flux distributions may stem directly from the merging of exponentially distributed cloud cores (Rasp et al., 2018, SC23). For simplicity, we chose however to ignore this fact to focus solely on the distributions of cloud mass fluxes.

Figure 11 shows cloud mass flux distributions obtained for all clouds identified at 2 km, 500 and 125 m resolutions. Best fits obtained with exponential and lognormal distributions using maximum likelihood estimation are also plotted. Cloud mass fluxes are close to being exponentially distributed as long as the density of clouds remains overall low and such that isolated cloud cores are unlikely to merge (i.e., at 2 km and 500 m resolution). In these cases, lognormal fits are visually as good as exponential ones, which is not a surprise given that the two-

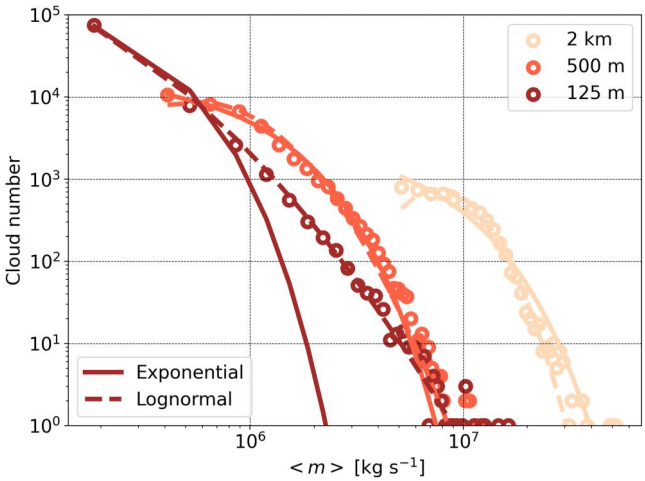

Figure 11. Empirical cloud mass flux distributions at 2 km, 500 and 125 m resolution (symbols) and corresponding best fits obtained using maximum likelihood estimation for exponential and lognormal distributions.

parameter lognormal distribution has a more flexible shape and is therefore expected to fit data ranging from nearly exponentially to nearly power-law distributed. As soon as cloud clustering and merging become significant, that is at 125 m resolution, the mass flux distribution displays a heavy tail. In this case, the empirical data can no longer be considered as being exponentially distributed, and it is best modeled using a lognormal function.

Overall, although the exponential distribution may still be considered as the best model in situations where weak organization is observed, the heavy tailed lognormal distribution should be preferred in organized cloud ensembles.

4.3. Total Mass Fluxes

Following the stochastic representation of convective cloud ensembles proposed by Craig and Cohen (2006), we are interested in modeling total mass flux fluctuations estimated across regions of varying sizes. The total mass flux within a region of a given size is simply equal to the sum of the mass fluxes of each cloud present in this region: $M = \sum_{i=1}^{N} m_i$. The distribution of total mass flux, denoted $h(M)$, therefore corresponds to the distribution of the random sum of N independent and identically distributed random variables m. Note that even though two clouds located in the same neighborhood are not completely independent if direct cloud-cloud interactions occur (i.e., if they are separated by less than ∼5 km), it is necessary here to assume complete statistical independence for the following computations to remain tractable.

In the previous sections, it was shown that N may be approximated by either a Poisson distribution f_P (spatial randomness) or a negative binomial distribution f_{NB} (spatial clustering), whereas m may be represented by either an exponential distribution g_E (isolated, non-interacting clouds) or a lognormal distribution g_{LN} (clustered clouds). Compounding these cloud count and mass flux distributions two by two, it is possible to design four different $h(M)$ models, which, in most cases, is not a trivial task: only in the situation where N is Poisson distributed and m exponentially distributed can we find an analytical solution, as in Craig and Cohen (2006). Consequently, in order to estimate $h(M)$, synthetic cloud populations must be generated by drawing N mass fluxes from either exponential or lognormal distributions, N following either a Poisson or a negative binomial distribution. This operation is repeated 10,000 times in each case to obtain meaningful statistics.

Figure 12 compares empirical and synthetic M distributions obtained at 2 km, 500 and 125 m, for block sizes of 4 km, 16 and 64 km. At 2 km resolution, no model based on negative binomial cloud counts could be constructed. The two remaining combinations of distributions are found to be equivalent independently of block size, in agreement with the fact that the cloud mass flux distribution at this resolution can be equally well fitted using exponential or lognormal functions. Increasing the horizontal grid length to 500 m, small differences become noticeable at block sizes ≥16 km (panels e and f), with the two models involving cloud counts drawn from negative binomials providing slightly more variability in M than the Poisson models. At this resolution, still no significant difference can be made between synthetic results simulated with exponentially and lognormally distributed mass fluxes.

In the most organized case at 125 m grid spacing, differences between the four models are more pronounced, although they still remain weak when considering block sizes of 4 km (panel g). In general, the model producing the worst synthetic results corresponds to the compound Poisson-exponential distribution. Deviations from the empirical data are particularly large at larger scales ($L_b = 64$ km) where the combination of Poisson and exponential distributions clearly underestimate the total mass flux variance. Considering lognormally distributed mass fluxes constitutes a slight upgrade over this basic model, but the more striking improvements are obtained when modeling cloud counts using a negative binomial distribution. This result illustrates the need to explicitly account for subgrid variability in cloud counts due to spatial organization.

To further quantify the deviations between empirical and synthetic M distributions, we introduce the Kullback-Leibler divergence D_{KL} measuring the distance between two distributions p and q as:

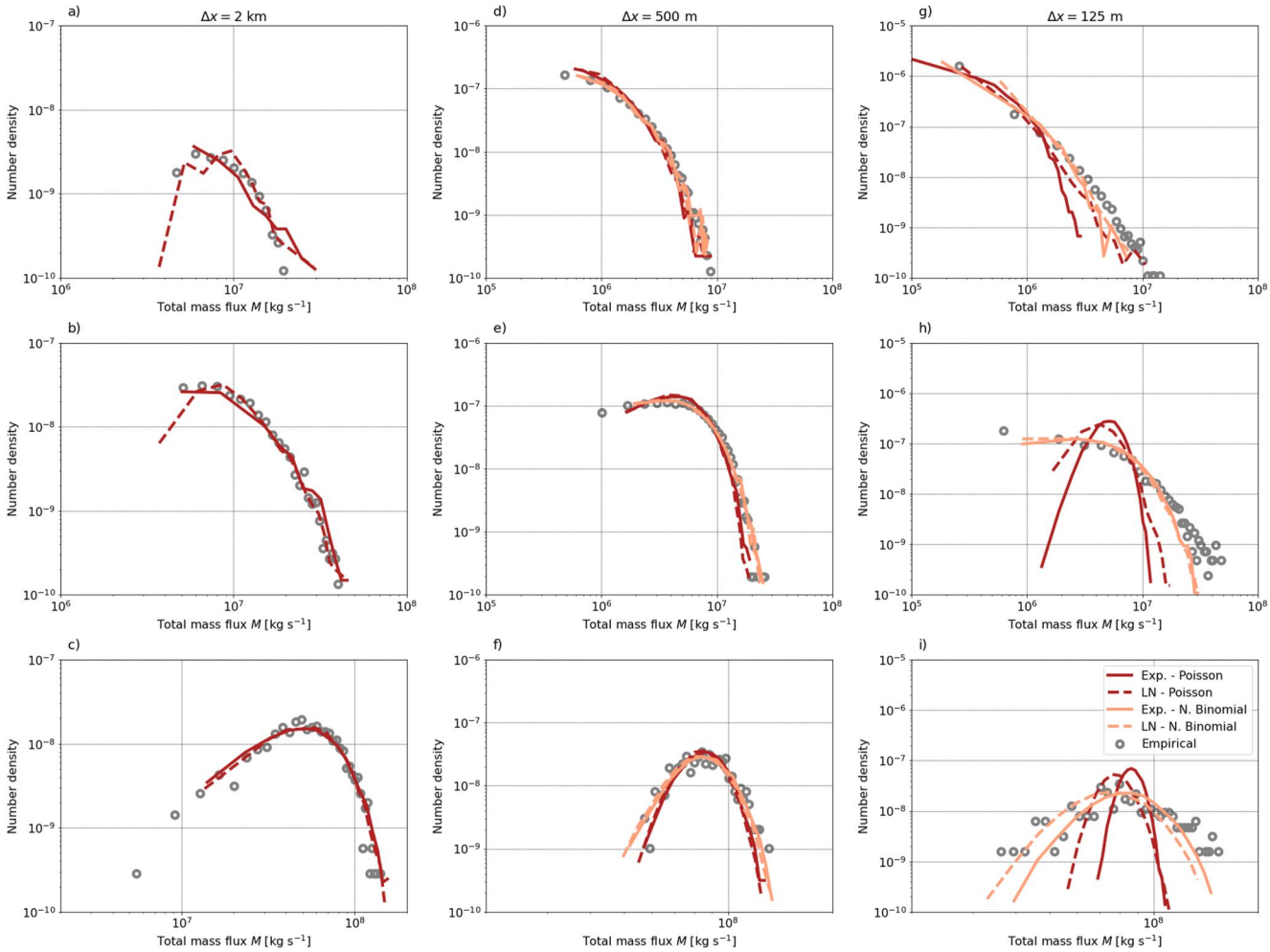

Figure 12. Empirical total mass flux distributions (symbols) displayed at (from left to right) 2 km, 500 and 125 m resolution and for box sizes of (from top to bottom) 4 km, 16 and 64 km. Solid and dashed lines represent synthetic distributions obtained by simulating cloud populations using combinations of either Poisson or negative binomial cloud counts, and either exponential or lognormal cloud mass fluxes.

$$D_{KL} = \sum_i p(x_i) \log\left[\frac{p(x_i)}{q(x_i)}\right], \tag{11}$$

where p stands for the empirical and q for the synthetic distributions, respectively. Figure 13 shows the dependence of D_{KL} on block size in the 125 m resolution case for all four statistical models tested. Furthermore, additional combinations were created corresponding to cloud counts or cloud mass fluxes held constant and equal to their block averages (all clouds and blocks are identical). This way, we can estimate how important it is to account for spatial fluctuations in cloud number and/or mas flux in organized convection and to parameterize them.

At small block sizes, in particular at $L_b < 4$ km, the best agreements between empirical and synthetic M distributions (lower D_{KL} values) are obtained when considering lognormally distributed mass fluxes, regardless of the cloud count distribution. The small number of clouds sampled within each block indeed makes the total mass flux fluctuations more sensitive to variations in cloud mass fluxes. Ignoring all variability in cloud number however yields very poor results, thus emphasizing the need to incorporate spatial cloud count fluctuations to adequately model the total mass flux distributions. In contrast, considering larger block sizes ($L_b > 8$ km), the best model combinations involve negative binomial distributions, independently of the mass flux distribution selected. In particular, at the largest block sizes, considering that clouds all have the same mass flux yields similar agreements

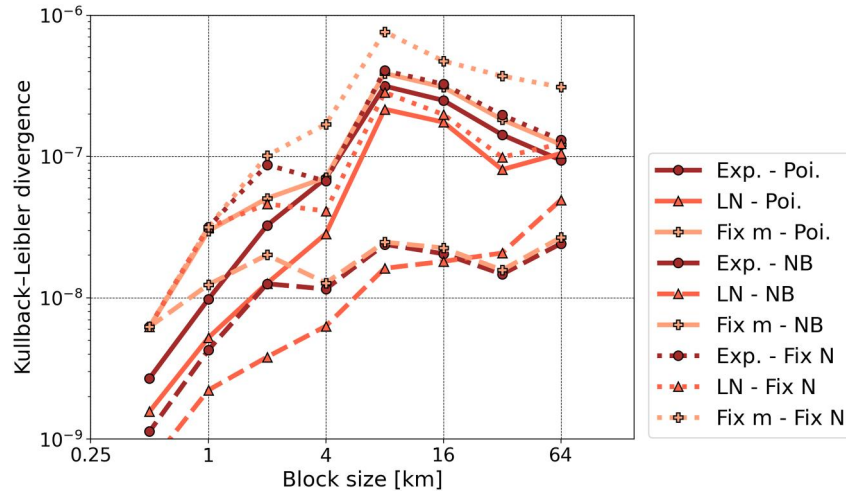

Figure 13. Kullback-Leibler divergence D_{KL} calculated by comparing empirical and simulated total mass flux distributions at different block sizes in the $\Delta x = 125$ m case. The four different combinations of distributions described in the text, as well as additional combinations involving a fixed mass flux per cloud or a fixed cloud count per block are represented.

with the empirical M distributions as more elaborate mass flux models. At these scales, the number of clouds sampled within each block is generally sufficient to provide a good representation of the overall cloud population, and fluctuations in individual cloud mass fluxes can to some extent be ignored.

The jump in D_{KL} observed on Figure 13 between 4 and 8 km may be interpreted as follows:

- At smaller scales, fluctuations in total mass flux depend primarily on the choice of the cloud mass flux distribution, and the benefit of choosing a heavy-tail mass flux model in situations of organized convection is evident,
- At larger scales, fluctuations in total mass flux are dominated by the cloud count variability and is therefore directly influenced by the spatial cloud arrangement.
- At all scales, accounting for the spatial variability in cloud number is crucial to represent fluctuations in total mass flux.

Interestingly, this scale separation also corresponds to the range of action of direct cloud-cloud interactions determined in Section 3.4. This agreement may be explained by the fact that at scales where direct interactions are relevant, cloud repulsion in regions of high cloud density tends to create random to regular cloud patterns characterized by low dispersion and therefore low cloud count variance. In contrast, the spatial cloud patterns observed at larger scales are a direct consequence of cold pool activity which results in enhanced cloud dispersion and cloud count variance. At these scales, the amount of clouds sampled depends on the presence/absence of cold pool gust fronts crossing the regions of interest.

5. Discussion

5.1. An Explanatory Stochastic Model of Organized Convection

In what follows, we wish to construct a simple conceptual model reflecting the very stochastic nature of organized cloud ensembles in an attempt to explain the statistical characteristics of the simulated cloud fields. As such, we wish to emphasize that the model presented does not incorporate elements that control the evolution of the cloud population in both time and space and thus does not include any memory effects.

In Section 3, it was shown that direct cloud-cloud interactions in organized RCE are only significant at short range, spatial cloud patterns being mostly controlled by heterogeneities in the probabilities to find clouds at particular locations (the cold pool fronts where moist static energy converges). Based on this result, we surmise that cloud patterns may be relatively well modeled using a heterogeneous point process whose point intensity is connected to the existence of cold pool fronts. In other words, clouds do not (or rarely) interact directly, but are randomly distributed along narrow bands of enhanced moist static energy along cold pool gust fronts. This model

therefore implies that clouds are always generated on the edges of existing cold pools, which constitutes a rather extreme view of spatial cloud organization since cloud organization is in general not solely driven by cold pool dynamics.

Based on these considerations, organized cloud fields may be fairly well represented using a class of point processes called Cox point processes (also known as doubly stochastic Poisson point processes). Cox point processes may be considered as a generalization of Poisson point processes where the intensity λ is itself defined as a stochastic spatial process. Using a Cox process in the present situation is hence a way to generate fully synthetic point populations without assuming a particular intensity distribution in order for the model to remain as general as possible. In particular, we may consider a subclass of Cox point processes in which the intensity is non zero along lines pseudo-randomly distributed in the plane, and zero everywhere else. This process may even be refined by letting the supporting lines be generated using Poisson-Voronoi tessellation. The resulting process may be created in three successive steps (Hirsch et al., 2019):

1. Randomly distribute N_p points in the plane (the seeds, obeying a HPPP): these points constitute the centers of mature cold pools distributed randomly in space;
2. Create the corresponding Voronoi diagram by delimiting cells containing all points in the plane closer to one of the N_p seeds than any other seed: each Voronoi cell represents an individual cold pool and the edges of the cell correspond to cold pool gust fronts along which moist static energy and moisture converge;
3. Randomly distribute N_c points along the edges of the Voronoi cells: these represent clouds developing randomly along the cold pool edges.

The resulting ensemble of N_c points follows a line Cox process.

Four realizations of this process are shown on Figure 14 for two different values of N_p and N_c, corresponding to low and high amounts of cold pools and clouds. The N_p Voronoi cells may be identified with N_p cold pools (the stochastic representation of cold pools using Poisson-Voronoi tessellation is reminiscent of the expanding circles model proposed by Haerter et al. (2019)), with N_c clouds developing randomly along their edges. Whereas it is out of the scope of the present study to provide an in-depth analysis of the patterns thus created, it is suggested that the line Cox point process constitutes an interesting framework to design conceptual models of cold pool driven convective organization.

As demonstrated by Hirsch et al. (2019), this particular class of Cox point processes percolates, meaning that properties generally associated with critical and sub-critical clusters in continuum percolation (Meester & Roy, 1996) apply. In particular, as the system of points distributed along the Voronoi cell edges approaches a critical threshold, the cluster size distribution is expected to develop a power-law tail. This analogy, may provide a credible explanation for the fact that power-law cloud size distributions have often been found in convective cloud ensembles (Benner & Curry, 1998; Heus & Seifert, 2013; Neggers et al., 2003; Savre & Craig, 2023a; van Laar et al., 2019; Welch et al., 1988), even when the cloud fraction is much smaller than the typical 2D continuum percolation threshold (~0.676 for disks). This idea is in particular supported by the recent results presented by Savre and Craig (2023a), in which power-law cloud size distributions were shown to emerge in cumulus cloud ensembles when individual cloud cores start to cluster and eventually merge to form bigger clouds.

5.2. Implications for Parameterizations

With stochastic convection parameterizations becoming increasingly popular, we wish to discuss if the results presented in Section 4 can provide relevant information for the design of such schemes.

First of all, it must be noted that the total mass flux variance was never found to be negligible at the scales analyzed (i.e., <100 km), which indicates that adding stochastic perturbations should always be required to correctly capture the variability in total mass flux at the subgrid scales. More interestingly, it was shown that the origin of these fluctuations actually varies depending on the scales considered. For grid boxes with areas $<5 \times 5$ km^2, only few clouds are found within each grid division and the cloud count variance remains small. The result is that fluctuations in total mass flux essentially follows the fluctuations in individual cloud mass flux. A similar conclusion was reached by Shutts and Palmer (2007) based on the theoretical formalism of Craig and Cohen (2006), as they determined that the total mass flux distribution across grid columns followed the individual mass flux distribution (assumed to be exponential), as long as the mean number of clouds per box remained ≤ 2. These conclusions were drawn based on a very different model configuration using a coarse horizontal resolution,

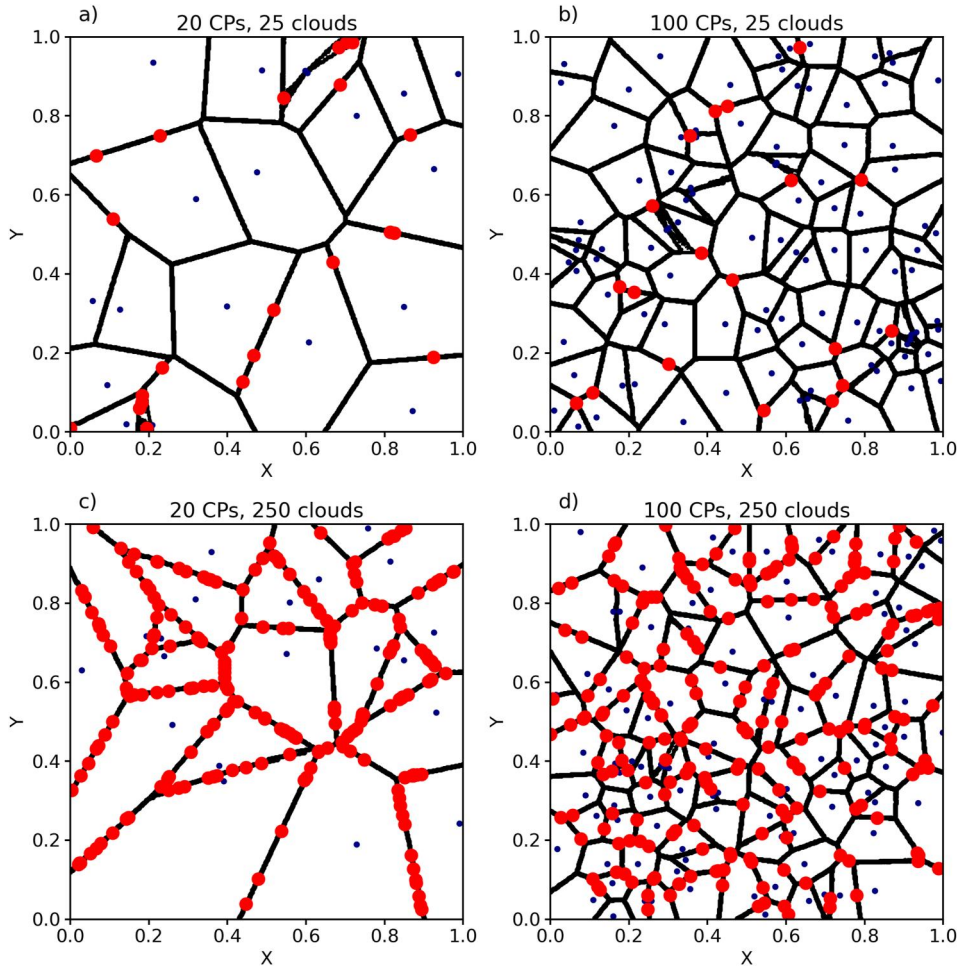

Figure 14. Four realizations of Cox point processes generated along lines defined as the edges of Poisson-Voronoi cells (the cold pools): (a) 20 cold pools and 25 clouds, (b) 100 cold pools and 25 clouds, (c) 20 cold pools and 250 clouds, and (d) 100 cold pools and 250 clouds. Dark blue dots indicate the location of the N_p randomly distributed seeds upon which each Voronoi diagram is constructed. Large red dots indicate the location of the N_c clouds randomly distributed along the Voronoi cell edges.

but a spatially varying forcing in a wider numerical domain. Despite these differences, it remains that accurately representing the individual cloud mass flux distribution in such situations appears to be essential.

In this context, it becomes especially critical to account for heavy-tailed mass flux distributions as observed in presence of strong organization. This problem was already recognized by Sakradzija et al. (2015, 2016) who suggested to use two Weibull distributions to parameterize the distribution of cloud mass fluxes. Using more elaborate mass flux distributions such as lognormal or Weibull distributions however increases the number of free parameters to be estimated by the model. Further work is then needed to constrain the shape of the mass flux distributions as in Sakradzija and Hohenegger (2017).

Considering larger boxes, the situation is reversed and variations in individual cloud mass flux may be neglected as long as the spatial cloud count variability is properly constrained. Fluctuations in cloud amount across grid columns were found to correlate strongly with the presence or absence of cold pool gust fronts. The result is an apparent enhancement of the cloud count variance, few to no clouds being sampled at the center of recovering cold pools, while a large amount of clouds may be found where cold pool fronts propagate and collide. This enhanced variability in cloud count was shown to be accurately modeled using a negative binomial distribution whose parameters can be related to local boundary layer activity. In this context, providing an accurate description of boundary layer organization at the subgrid scales appears to be particularly critical, especially considering that

even models operating at kilometer scales are not able to represent them sufficiently well. This view supports ideas emphasizing the representation of subgrid cold pool activity as in Qian et al. (1998), Grandpeix and Lafore (2010), or Mapes and Neale (2011).

6. Conclusion

Spatial organization is one of the main processes that is still misrepresented in modern convection parameterizations. In an attempt to provide guidance for the design of models capable of representing organized convection, idealized RCE simulations performed at resolutions ranging from 2 km to 125 m (exhibiting from perfectly random to highly organized cloud patterns) were analyzed. The main objectives were to characterize in detail the simulated spatial cloud patterns, and to develop a statistical description of the convective cloud ensembles capable of predicting the fluctuations in convective mass flux at various scales.

A comprehensive analysis of the spatial cloud patterns led to the conclusion that cloud ensembles in such organized RCE simulations may be adequately represented by heterogeneous point processes in which clouds do not interact directly substantially, but align randomly along cold pool gust fronts. Direct interactions (repulsion) may still occur, but these are relatively short range and act only at scales <5 km in the highest resolution simulations. At larger scales, cloud patterns are almost entirely controlled by spatial heterogeneities in boundary layer moist static energy that reflect the presence and dynamics of cold pools. This conclusion is somehow similar to Colin et al. (2019) insofar as the memory of past convective activity stored in the boundary layer state controls to a large extent the spatial organization of the cloud population.

We then focused on the total mass flux simulated within square quadrats of varying sizes (using a coarse graining approach), which is essentially the result of a random sum of random mass fluxes. In this context, both the distributions of cloud mass fluxes and cloud counts sampled within quadrats of given sizes were characterized. Whereas our results agree with the statistical mechanics theory of Craig and Cohen (2006) in perfectly random situations (i.e., at coarse resolution), the development of new models to represent cloud count and mass flux distributions becomes necessary when the degree of spatial organization increases. The negative binomial distribution was shown to accurately represent cloud count overdispersion under organized conditions where the cloud count variance can exceed that expected in completely random situations. In addition, the lognormal distribution was chosen as an adequate model able to represent the heavy tails of the mass flux distributions obtained in organized conditions.

It was shown that using a negative binomial count with lognormal mass fluxes provides the best agreement with the empirical total mass flux distributions sampled at all scales. Simpler models were however found to yield equally good results at specific scales. For box sizes <5 km, total mass flux fluctuations were found to be primarily controlled by the large variance in mass flux per cloud such that it is, at these scales, particularly important to model the heavy tails of the mass flux distributions (using for example a lognormal function). Drawing the subgrid cloud count from a simple Poisson distribution suffices because of the absence of clustering at small scales. Considering box sizes >5 km, the situation is reversed and it is essential to explicitly account for overdispersion in cloud count across boxes in order to represent fluctuations in total mass flux per box. The heavy tails of the mass flux distributions can however be ignored in this situation.

In this study, we chose to focus on particular aspects of the spatial organization of convective clouds, and a particular representation of fluctuations in the simulated cloud ensembles. As such, we acknowledge that several important related questions were omitted and that we ignored some of the simplifications that the idealized RCE setup implies. Among the issues that have not been addressed, we would like to emphasize the following:

1. The statistical description of organized convection discussed here requires the estimation of various parameters that are a priori not known. Designing more sophisticated and more accurate statistical models indeed comes at the expense of having to constrain an increasingly large number of parameters, from two in the simple equilibrium model described by Craig and Cohen (2006) to four in the most complex case proposed here. For example, one important parameter that needs to be constrained is the mean mass flux per cloud. Whereas Plant and Craig (2008) suggested that this quantity may be set to a constant, other studies have noted the importance of choosing a variable mean mass flux and have tried to relate this quantity to various atmospheric properties (Sakradzija & Hohenegger, 2017). Furthermore, in order to estimate the extra parameters required to fully parameterize the total mass flux variability, it appears primordial to incorporate information regarding the

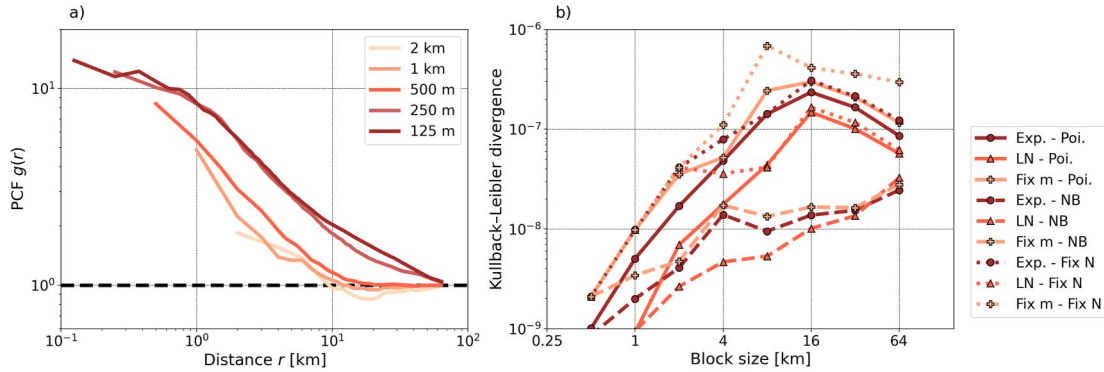

Figure 15. (a) Reproduction of Figure 4a, this time with clouds identified at an altitude of 2,400 m (instead of 1,275 m) above the surface. (b) Reproduction of Figure 13, again with clouds identified at an altitude of 2,400 m.

organization state of the cloud ensemble. Although some solutions have been proposed in the past to parameterize convective organization at the mesoscales (Mapes & Neale, 2011; Moncrieff et al., 2017), to our knowledge, no concrete approach has yet been developed and successfully tested. Further work is required in this direction to characterize the dependency of these parameters on external factors.

2. An other issue concerns the fact the smallest clouds sampled and analyzed in this study (and any similar one) are necessarily as big as the numerical grid. These small clouds are of course impacted by the numerical resolution and they are likely not realistically represented by the model, although they contribute to the total mass flux, and thus to the equilibrium state. Ignoring them would create a certain imbalance, especially since they dominate the overall cloud count, but including them (which we chose to do here) introduces statistical biases affecting in particular the estimated mean cloud number and mean mass flux. We may consequently wonder about the size of the smallest clouds relevant to the parameterization problem, and, perhaps more importantly, about the numerical configuration needed to simulate a realistic cloud ensemble.
3. We should also question the importance of the quasi-equilibrium assumption on our results. Quasi-equilibrium is indeed at the heart of the mass flux concept used to parameterize convection, and it holds almost exactly everywhere and at any time in the analysis presented here. Departures from quasi-equilibrium may however occur in practice when the forcing varies at time scales smaller than the convective adjustment time scale (Yano & Plant, 2012). Convection and its organization may then respond differently compared to the equilibrium situation addressed in this work. At this point, theoretical and statistical descriptions of convective cloud ensembles under out-of-equilibrium situations are still missing.
4. Finally, we should stress the fact that the idealized configuration used in this study limited the analysis to a certain type of self-organization driven almost exclusively by cold pool dynamics. The results presented may therefore not be representative of convective organization in general, and may differ when considering, for example, the convective self-aggregation mechanism described in Muller and Held (2012) or Muller and Bony (2015).

Appendix A: Sensitivity to the Cloud Identification Altitude

All results presented in this manuscript were produced identifying clouds at an altitude of 1,275 m above the surface. At this altitude, most shallow and deep clouds are sampled and virtually no cloud is left out of the analysis. One may thus wonder if this choice has any influence on the results and if identifying clouds at higher altitudes changes our conclusions. This question is addressed in the following where part of the analysis has been redone with clouds identified at an altitude of 2,400 m.

Regardless of horizontal grid spacing, less than half of the clouds identified at 1,275 m are still present at 2,400 m thus indicating that a large fraction of the total cloud population is effectively excluded from the analysis at the higher altitude. Despite this, no particular difference in the spatial organization of the cloud population between 1,275 m and 2,400 m can be discerned. For example, Figure 15a shows the overall PCFs computed at horizontal grid spacings ranging from 2 km to 125 m for clouds identified at 2,400 m. Figure 15a displays the same characteristics as Figure 4a, with clustering at short scales but spatial randomness at distances >10 km at grid

lengths of 2 km–500 m, and long range correlations and overall clustering at smaller grid spacings. Other measures of clustering and spatial organization (like the index of dispersion I_d) exhibit the same similarities at 1,275 m and 2,400 m.

Provided that the spatial organization of the cloud population is similar at 1,275 m and 2,400 m, the cloud count within subregions of varying sizes can be equally well represented using negative binomial distributions in both cases. In particular, modeling the total mass flux within these subregions using combinations of different mass flux and cloud count distributions yields the same conclusions at both 1,275 m and 2,400 m. As shown on Figure 15b (to be compared with Figure 13), it appears indeed that introducing overdispersion in the parameterized cloud count using negative binomial distributions is particularly crucial to accurately represent the total mass flux within subregions of sizes larger than 4 km, but parameterizing the heavy tail of the mass flux distributions (using lognormal distributions) becomes equally, if not more important at smaller scales.

Overall, these results indicate that our conclusions are not affected by the altitude at which clouds are identified and hold whether the shallowest clouds in the domain are included in the analysis or not.

Data Availability Statement

The data used in this manuscript was generated using the MIMICA model, available at the following address: https://bitbucket.org/matthiasbrakebusch/mimicav5/src/master/ (Savre & Brakebusch, 2024). The complete data set was previously described in Savre and Craig (2023b) and can be accessed via the Open Data LMU server: https://doi.org/10.5282/ubm/data.321 (Savre & Craig, 2022).

Acknowledgments
The Gauss Centre for Supercomputing e.V. is gratefully acknowledged for providing computing time on the GCS Supercomputer SuperMUC at Leibniz Supercomputing Centre (LRZ). The author would also like to thank G. Craig who suggested the initial idea onto which this work is based, as well as T. Kostenbader for his help in setting up and evaluating some of the analyses presented in this paper. Open Access funding enabled and organized by Projekt DEAL.

References

Arakawa, A., & Schubert, W. (1974). Interaction of a cumulus cloudensemble with the large-scale environment, Part I. *Journal of the Atmospheric Sciences*, *31*(3), 674–701. https://doi.org/10.1175/1520-0469(1974)031⟨0674:IOACCE⟩2.0.CO;2

Baddeley, A., Rubak, E., & Turner, R. (2015). *Spatial point patterns: Methodology and applications with R* (1st ed.). Chapman and Hall/CRC. https://doi.org/10.1201/b19708

Bengtsson, L., Steinheimer, M., Bechtold, P., & Geleyn, J.-F. (2013). A stochastic parametrization for deep convection using cellular automata. *Quarterly Journal of the Royal Meteorological Society*, *139*(675), 1533–1543. https://doi.org/10.1002/qj.2108

Benner, T., & Curry, J. (1998). Characteristics of small tropical cumulus clouds and their impact on the environment. *Journal of Geophysical Research*, *27*(D22), 28753–28767. https://doi.org/10.1029/98jd02579

Biagioli, G., & Tompkins, A. M. (2023). A dimensionless parameter for predicting convective self-aggregation onset in a stochastic reaction-diffusion model of tropical radiative-convective equilibrium. *Journal of Advances in Modeling Earth Systems*, *15*(5), e2022MS003231. https://doi.org/10.1029/2022MS003231

Bliss, C. I., & Fisher, R. A. (1953). Fitting the negative binomial distribution to biological data. *Biometrics*, *9*(2), 176–200. https://doi.org/10.2307/3001850

Bony, S., Stevens, B., Frierson, D. e. a., Jakob, C., Kageyama, M., Pincus, R., et al. (2015). Circulation and climate sensitivity. *Nature*, *8*(4), 261–268. https://doi.org/10.1038/ngeo2398

Bretherton, C. S., Blossey, P. N., & Khairoutdinov, M. (2005). An energy-balance analysis of deep convective self-aggregation above uniform sst. *Journal of the Atmospheric Sciences*, *62*(12), 4273–4292. https://doi.org/10.1175/JAS3614.1

Chandra, A. S., Zuidema, P., Krueger, S., Kochanski, A., de Szoeke, S. P., & Zhang, J. (2018). Moisture distributions in tropical cold pools from equatorial Indian Ocean observations and cloud-resolving simulations. *Journal of Geophysical Research: Atmospheres*, *123*(20), 11445–-11465. https://doi.org/10.1029/2018JD028634

Cohen, B. G., & Craig, G. C. (2006). Fluctuations in an equilibrium convective ensemble. Part II: Numerical experiments. *Journal of the Atmospheric Sciences*, *63*(8), 2005–2015. https://doi.org/10.1175/JAS3710.1

Colin, M., Sherwood, S., Geoffroy, O., Bony, S., & Fuchs, D. (2019). Identifying the sources of convective memory in cloud-resolving simulations. *Journal of the Atmospheric Sciences*, *76*(3), 947–962. https://doi.org/10.1175/JAS-D-18-0036.1

Coppin, D., & Bony, S. (2015). Physical mechanisms controlling the initiation of convective self-aggregation in a general circulation model. *Journal of Advances in Modeling Earth Systems*, *7*(4), 2060–2078. https://doi.org/10.1002/2015MS000571

Craig, G. C., & Cohen, B. G. (2006). Fluctuations in an equilibrium convective ensemble. Part I: Theoretical formulation. *Journal of the Atmospheric Sciences*, *63*(8), 1996–2004. https://doi.org/10.1175/JAS3709.1

Davoudi, D., McFarlane, N. A., & Birner, T. (2010). Fluctuation of mass flux in a cloud-resolving simulation with interactive radiation. *Journal of the Atmospheric Sciences*, *67*(2), 400–418. https://doi.org/10.1175/2009JAS3215.1

de Szoeke, S. P., Skyllingstad, E. D., Zuidema, P., & Chandra, A. S. (2017). Cold pools and their influence on the tropical marine boundary layer. *Journal of the Atmospheric Sciences*, *74*(4), 1149–1168. https://doi.org/10.1175/JAS-D-16-0264.1

Diggle, P. J. (2014). *Statistical analysis of spatial and spatio-temporal point patterns* (3rd ed.). Chapman and Hall/CRC. https://doi.org/10.1201/b15326

Feng, Z., Hagos, S., Rowe, A. K., Burleyson, C. D., Martini, M. N., & de Szoeke, S. P. (2015). Mechanisms of convective cloud organization by cold pools over tropical warm ocean during the AMIE/DYNAMO field campaign. *Journal of Advances in Modeling Earth Systems*, *7*(2), 357–381. https://doi.org/10.1002/2014MS000384

Grabowski, W. W. (1998). Toward cloud resolving modeling of large-scale tropical circulations: A simple cloud microphysics parameterization. *Journal of the Atmospheric Sciences*, *55*(21), 3283–3298. https://doi.org/10.1175/1520-0469(1998)055⟨3283:TCRMOL⟩2.0.CO;2

Grandpeix, J.-Y., & Lafore, J.-P. (2010). A density current parameterization coupled with Emanuel's convection scheme. Part I: The models. *Journal of the Atmospheric Sciences*, *67*(4), 881–897. https://doi.org/10.1175/2009JAS3044.1

Haerter, J. O., Böing, S. J., Henneberg, O., & Nissen, S. B. (2019). Circling in on convective organization. *Geophysical Research Letters*, *46*(12), 7024–7034. https://doi.org/10.1029/2019GL082092

Hagos, S., Feng, Z., Plant, R. S., Houze, R. A., Jr., & Xiao, H. (2018). A stochastic framework for modeling the population dynamics of convective clouds. *Journal of Advances in Modeling Earth Systems*, *10*(2), 448–465. https://doi.org/10.1002/2017MS001214

Held, I. M., Hemler, R. S., & Ramaswamy, V. (1993). Radiative-convective equilibrium with explicit two-dimensional moist convection. *Journal of the Atmospheric Sciences*, *50*(23), 3909–3927. https://doi.org/10.1175/1520-0469(1993)050⟨3909:RCEWET⟩2.0.CO;2

Heus, T., & Seifert, A. (2013). Automated tracking of shallow cumulus clouds in large domain, long duration large-eddy simulations. *Geoscientific Model Development*, *6*(4), 1261–1273. https://doi.org/10.5194/gmd-6-1261-2013

Hirsch, C., Jahnel, B., & Cali, E. (2019). Continuum percolation for cox point processes. *Stochastic Processes and their Applications*, *129*(10), 3941–3966. https://doi.org/10.1016/j.spa.2018.11.002

Hohenegger, C., & Stevens, B. (2016). Coupled radiative convective equilibrium simulations with explicit and parameterized convection. *Journal of Advances in Modeling Earth Systems*, *8*(3), 1468–1482. https://doi.org/10.1002/2016MS000666

Holloway, C. E., & Woolnough, S. J. (2016). The sensitivity of convective aggregation to diabatic processes in idealized radiative-convective equilibrium simulations. *Journal of Advances in Modeling Earth Systems*, *8*(1), 166–195. https://doi.org/10.1002/2015MS000511

Houze, R. A., Jr. (2004). Mesoscale convective systems. *Reviews of Geophysics*, *42*(4). https://doi.org/10.1029/2004RG000150

Jeevanjee, N., & Romps, D. M. (2013). Convective self-aggregation, cold pools, and domain size. *Geophysical Research Letters*, *40*(5), 994–998. https://doi.org/10.1002/grl.50204

Jordan, C. L. (1958). Mean soundings for the West Indies area. *Journal of the Atmospheric Sciences*, *15*(1), 91–97. https://doi.org/10.1175/1520-0469(1958)015⟨0091:MSFTWI⟩2.0.CO;2

Keane, R. J., Craig, G. C., Keil, C., & Zängl, G. (2014). The plant-craig stochastic convection scheme in icon and its scale adaptivity. *Journal of the Atmospheric Sciences*, *71*(9), 3404–3415. https://doi.org/10.1175/JAS-D-13-0331.1

Khairoutdinov, M. F., Krueger, S. K., Moeng, C.-H., Bogenschutz, P. A., & Randall, D. A. (2009). Large-eddy simulation of maritime deep tropical convection. *Journal of Advances in Modeling Earth Systems*, *1*(4). https://doi.org/10.3894/JAMES.2009.1.15

Khouider, B., Biello, J., & Majda, A. (2010). A stochastic multicloud model for tropical convection. *Communications in Mathematical Sciences*, *8*(1), 187–216. https://doi.org/10.4310/cms.2010.v8.n1.a10

Lebo, Z. J., & Morrison, H. (2015). Effects of horizontal and vertical grid spacing on mixing in simulated squall lines and implications for convective strength and structure. *Monthly Weather Review*, *143*(11), 4355–4375. https://doi.org/10.1175/MWR-D-15-0154.1

LeMone, M. A., & Zipser, E. J. (1980). Cumulonimbus vertical velocity events in gate. Part I: Diameter, intensity and mass flux. *Journal of the Atmospheric Sciences*, *37*(11), 2444–2457. https://doi.org/10.1175/1520-0469(1980)037⟨2444:CVVEIG⟩2.0.CO;2

Mapes, B., & Neale, R. (2011). Parameterizing convective organization to escape the entrainment dilemma. *Journal of Advances in Modeling Earth Systems*, *3*(2), M06004. https://doi.org/10.1029/2011ms000042

Mauritsen, T., & Stevens, B. (2015). Missing iris effect as a possible cause of muted hydrological change and high climate sensitivity in models. *Nature Geoscience*, *8*(5), 346–351. https://doi.org/10.1038/ngeo2414

Meester, R., & Roy, R. (1996). *Continuum percolation* (1st ed.). Cambridge University Press. https://doi.org/10.1017/CBO9780511895357

Moncrieff, M. W., Liu, C., & Bogenschutz, P. (2017). Simulation, modeling, and dynamically based parameterization of organized tropical convection for global climate models. *Journal of the Atmospheric Sciences*, *74*(5), 1363–1380. https://doi.org/10.1175/JAS-D-16-0166.1

Muller, C. J., & Bony, S. (2015). What favors convective aggregation and why? *Geophysical Research Letters*, *42*(13), 5626–5634. https://doi.org/10.1002/2015GL064260

Muller, C. J., & Held, I. M. (2012). Detailed investigation of the self-aggregation of convection in cloud-resolving simulations. *Journal of the Atmospheric Sciences*, *69*(8), 2551–2565. https://doi.org/10.1175/JAS-D-11-0257.1

Nair, U. S., Weger, R. C., Kuo, K. S., & Welch, R. M. (1998). Clustering, randomness and regularity in cloud fields 5. the nature of regular cumulus cloud fields. *Journal of Geophysical Research*, *103*(D10), 11363–11380. https://doi.org/10.1029/98jd00088

Neggers, R. A. J., Jonker, H. J. J., & Siebesma, A. (2003). Size statistics of cumulus cloud populations in large-eddy simulations. *Journal of the Atmospheric Sciences*, *60*(8), 1060–1074. https://doi.org/10.1175/1520-0469(2003)60

Pendergrass, A. G., Reed, K. A., & Medeiros, B. (2016). The link between extreme precipitation and convective organization in a warming climate: Global radiative-convective equilibrium simulations. *Geophysical Research Letters*, *43*(21), 11445–11452. https://doi.org/10.1002/2016GL071285

Plant, R. S., & Craig, G. C. (2008). A stochastic parameterization for deep convection based on equilibrium statistics. *Journal of the Atmospheric Sciences*, *65*(1), 87–105. https://doi.org/10.1175/2007JAS2263.1

Prein, A. F., Rasmussen, R. M., Wang, D., & Giangrande, S. E. (2021). Sensitivity of organized convective storms to model grid spacing in current and future climates. *Philosophical Transactions of the Royal Society A*, *379*(2195), 20190546. https://doi.org/10.1098/rsta.2019.0546

Qian, L., Young, G. S., & Frank, W. M. (1998). A convective wake parameterization scheme for use in general circulation models. *Monthly Weather Review*, *126*(2), 456–469. https://doi.org/10.1175/1520-0493(1998)126⟨0456:ACWPSF⟩2.0.CO;2

Rasp, S., Selz, T., & Craig, G. C. (2018). Variability and clustering of midlatitude summertime convection: Testing the Craig and Cohen theory in a convection-permitting ensemble with stochastic boundary layer perturbations. *Journal of the Atmospheric Sciences*, *75*(2), 691–706. https://doi.org/10.1175/JAS-D-17-0258.1

Rio, C., Del Genio, A. D., & Hourdin, F. (2019). Ongoing breakthrough in convective parameterization. *Current Climate Change Reports*, *5*(2), 95–111. https://doi.org/10.1007/s40641-019-00127-w

Rotunno, R., Klemp, J. B., & Weismann, M. L. (1988). A theory for strong, long-lived squall lines. *Journal of the Atmospheric Sciences*, *45*(3), 463–485. https://doi.org/10.1175/1520-0469(1988)045⟨0463:ATFSLL⟩2.0.CO;2

Sakradzija, M., & Hohenegger, C. (2017). What determines the distribution of shallow convective mass flux through a cloud base? *Journal of the Atmospheric Sciences*, *74*(8), 2615–2632. https://doi.org/10.1175/jas-d-16-0326.1

Sakradzija, M., Seifert, A., & Dipankar, A. (2016). A stochastic scale-aware parameterization of shallow cumulus convection across the convective gray zone. *Journal of Advances in Modeling Earth Systems*, *7*(2), 786–812. https://doi.org/10.1002/2016MS000634

Sakradzija, M., Seifert, A., & Heus, T. (2015). Fluctuations in a quasi-stationary shallow cumulus cloud ensemble. *Nonlinear Processes in Geophysics*, *22*(1), 65–85. https://doi.org/10.5194/npg-22-65-2015

Savre, J., & Brakebusch, M. (2024). MIMICAV5 [Software]. *bitbucket*. https://bitbucket.org/matthiasbrakebusch/mimicav5/src/master/

Savre, J., & Craig, G. (2022). Dataset presented in the manuscript the sensitivity of convective cloud ensemble statistics to horizontal resolution in idealized RCE simulations [Dataset]. *Open Data LMU*. https://doi.org/10.5282/ubm/data.321

Savre, J., & Craig, G. (2023a). Fitting cumulus cloud size distributions from idealized cloud resolving model simulations. *Journal of Advances in Modeling Earth Systems*, *15*(5), e2022MS003360. https://doi.org/10.1029/2022MS003360

Savre, J., & Craig, G. (2023b). The sensitivity of convective cloud ensemble statistics to horizontal grid spacing in idealized rce simulations. *Journal of the Atmospheric Sciences*, *83*(5), 1267–1284. https://doi.org/10.1175/JAS-D-22-0164.1

Savre, J., Ekman, A. M. L., & Svensson, G. (2014). Technical note: Introduction to MIMICA, a large-eddy simulation solver for cloudy planetary boundary layers. *Journal of Advances in Modeling Earth Systems*, *6*(3), 630–649. https://doi.org/10.1002/2013MS000292

Senf, F., Brueck, M., & Klocke, D. (2019). Pair correlations and spatial statistics of deep convection over the tropical Atlantic. *Journal of the Atmospheric Sciences*, *76*(10), 3211–3228. https://doi.org/10.1175/JAS-D-18-0326

Shin, J., & Park, S. (2020). A stochastic unified convection scheme (UNICON). Part I: Formulation and single-column simulation for shallow convection. *Journal of the Atmospheric Sciences*, *77*(2), 583–610. https://doi.org/10.1175/JAS-D-19-0117.1

Shutts, G. J., & Palmer, T. N. (2007). Convective forcing fluctuations in a cloud-resolving model: Relevance to the stochastic parameterization problem. *Journal of Climate*, *20*(2), 187–202. https://doi.org/10.1175/JCLI3954.1

Squitieri, B. J., & Gallus, W. A., Jr. (2022). On the changes in convection-allowing WRF forecasts of MCS evolution due to decreases in model horizontal and vertical grid spacing. Part I: Changes in cold pool evolution. *Weather and Forecasting*, *37*(10), 1903–1923. https://doi.org/10.1175/WAF-D-22-0041.1

Stoyan, D., & Stoyan, H. (1994). *Fractals, random shapes, and point fields: Methods of geometrical statistics*. John Wiley & Sons.

Sueki, K., Yamaura, T., Yashiro, H., Nishizawa, S., Yoshida, R., Kajikawa, Y., & Tomita, H. (2019). Convergence of convective updraft ensembles with respect to the grid spacing of atmospheric models. *Geophysical Research Letters*, *46*(24), 14817–14825. https://doi.org/10.1029/2019GL084491

Tan, J., Jakob, C., Rossow, W. B., & Tselioudis, G. (2015). Increases in tropical rainfall driven by changes in frequency of organized deep convection. *Nature*, *519*(7544), 451–454. https://doi.org/10.1038/nature14339

Tobin, I., Bony, S., & Roca, R. (2012). Observational evidence for relationships between the degree of aggregation of deep convection, water vapor, surface fluxes, and radiation. *Journal of Climate*, *25*(20), 6885–6904. https://doi.org/10.1175/jcli-d-11-00258.1

Tompkins, A. M. (2001a). Organization of tropical convection in low vertical wind shears: The role of cold pools. *Journal of the Atmospheric Sciences*, *58*(13), 1650–1672. https://doi.org/10.1175/1520-0469(2001)058<1650:OOTCIL>2.0.CO;2

Tompkins, A. M. (2001b). Organization of tropical convection in low vertical wind shears: The role of water vapor. *Journal of the Atmospheric Sciences*, *58*(6), 529–545. https://doi.org/10.1175/1520-0469(2001)058<0529:OOTCIL>2.0.CO;2

Tompkins, A. M., & Craig, G. C. (1998). Radiative–convective equilibrium in a three-dimensional cloud-ensemble model. *Quarterly Journal of the Royal Meteorological Society*, *124*(550), 2073–2097. https://doi.org/10.1002/qj.49712455013

Tompkins, A. M., & Semie, A. G. (2017). Organization of tropical convection in low vertical wind shears: Role of updraft entrainment. *Journal of Advances in Modeling Earth Systems*, *9*(2), 1046–1068. https://doi.org/10.1002/2016MS000802

Torri, G., Kuang, Z., & Tian, Y. (2015). Mechanisms for convection triggering by cold pools. *Geophysical Research Letters*, *42*(6), 1943–1950. https://doi.org/10.1002/2015GL063227

van Laar, T. W., Schemann, V., & Neggers, R. A. J. (2019). Investigating the diurnal evolution of the cloud size distribution of continental cumulus convection using multiday LES. *Journal of the Atmospheric Sciences*, *767*(3), 729–747. https://doi.org/10.1175/JAS-D-18-0084.1

Ver Hoef, P., & Boveng, J. (2007). Quasi-Poisson vs. negative binomial regression: How should we model overdispersed count data? *Ecology*, *88*(11), 2766–2772. https://doi.org/10.1890/07-0043.1

Villarini, G., Vecchi, G., & Smith, J. (2010). Modeling of the dependence of tropical storm counts in the North Atlantic basin on climate indices. *Monthly Weather Review*, *138*(7), 2681–2705. https://doi.org/10.1175/2010MWR3315.1

Welch, R., Kuo, K., Wielicki, B., Sengupta, S., & Parker, L. (1988). Marine stratocumulus cloud fields off the coast of southern California observed using LANDSAT imagery. Part I: Structural characteristics. *Journal of Applied Meteorology and Climatology*, *27*(4), 341–362. https://doi.org/10.1175/1520-0450(1988)027<0341:mscfot>2.0.co;2

Wing, A. A., Stauffer, C. L., Becker, T., Reed, K. A., Ahn, M.-S., Arnold, N. P., et al. (2020). Clouds and convective self-aggregation in a multimodel ensemble of radiative-convective equilibrium simulations. *Journal of Advances in Modeling Earth Systems*, *12*(9), e2020MS002138. https://doi.org/10.1029/2020MS002138

Yanai, M., Esbensen, S., & Chu, J.-H. (1973). Determination of bulk properties of tropical cloud clusters from large-scale heat and moisture budgets. *Journal of the Atmospheric Sciences*, *30*(4), 611–627. https://doi.org/10.1175/1520-0469(1973)030⟨0611:DOBPOT⟩2.0.CO;2

Yanase, T., Nishizawa, S., Miura, H., Takemi, T., & Tomita, H. (2020). New critical length for the onset of self-aggregation of moist convection. *Geophysical Research Letters*, *47*(16), e2020GL088763. https://doi.org/10.1029/2020GL088763

Yang, B., Wang, M., Zhang, G. J., Guo, Z., Wang, Y., Xu, X., et al. (2022). Parameterizing convective organization effects with a moisture-pdf approach in climate models: Concept and a regional case simulation. *Journal of Advances in Modeling Earth Systems*, *14*(5), e2021MS002942. https://doi.org/10.1029/2021MS002942

Yano, J.-I., & Plant, R. S. (2012). Convective quasi equilibrium. *Reviews of Geophysics*, *50*(4), RG4004. https://doi.org/10.1029/2011RG000378

References From the Supporting Information

Lipps, F. B., & Hemler, R. S. (1982). A scale analysis of deep moist convection and some related numerical calculations. *Journal of the Atmospheric Sciences*, *39*(10), 2192–2210. https://doi.org/10.1175/1520-0469(1982)039h2192:ASAODMi2.0.CO;2

Morinishi, Y., Lund, T. S., Vasilyev, O. V., & Moin, P. (1998). Fully conservative high order finite difference schemes for incompressible flow. *Journal of Computational Physics*, *143*, 90–124.

Smagorinsky, J. (1963). General circulation experiments with the primitive equations: 1. the basic experiment. *Monthly Weather Review*, *911*, 99–164.

van Leer, B. (1979). Towards the ultimate conservative difference scheme v. a second order sequel to Godunov's method. *Journal of computational Physics*, *32*(1), 101–136. https://doi.org/10.1016/0021-9991(79)90145-1

Zuidema, P., Torri, G., Muller, C., & Chandra, A. (2017). A survey of precipitation induced atmospheric cold pools over oceans and their interactions with the larger scale environment. *Surveys in Geophysics*, *38*, 1283–1305. https://doi.org/10.1007/s10712-017-944